

Direct imaging of exoplanets

Alice Zurlo^{a,b}

^aInstituto de Estudios Astrofísicos, Facultad de Ingeniería y Ciencias, Universidad Diego Portales, Av. Ejército Libertador 441, Santiago, Chile

^bMillennium Nucleus on Young Exoplanets and their Moons (YEMS)

© 20xx Elsevier Ltd. All rights reserved.

Chapter Article tagline: update of previous edition, reprint..

Nomenclature

4QPM	Four quadrant phase-mask
ADI	Angular Differential Imaging
ALC	Apodized Lyot Coronagraph
AO	Adaptive Optics
APP	Apodizing phase plate
au	Astronomical Unit
BD	Brown Dwarf
CA	Core Accretion
DM	Deformable Mirror
eELT	European Extremely Large Telescope
ERIS	Enhanced Resolution Imager and Spectrograph
FOV	Field Of View
GI	Gravitational Instability
HCI	High-Contrast Imaging
JWST	James Webb Space Telescope
IWA	Inner Working Angle
LOCI	Locally Optimized Combination of Images
NACO	NAos CONica
NIR	Near-Infrared
OWA	Outer Working Angle
PCS	Planetary Camera and Spectrograph
PSF	Point Spread Function
RDI	Reference Differential Imaging
RV	Radial Velocity
SDI	Spectral Differential Imaging
SNR	Signal-to-Noise Ratio
SPHERE	Spectro-Polarimetric High-contrast Exoplanet REsearch
SR	Strehl Ratio
VLT	Very Large Telescope
VLTI	Very Large Telescope Interferometer

Glossary

Adaptive optics systems: Adaptive optics systems enhance ground-based telescopes' resolution by correcting atmospheric turbulence, enabling clearer observations of celestial objects.

Airy Disk: In optics, particularly in telescopes, the Airy disk refers to the central bright disk surrounded by concentric rings in the image of a point source of light. It is a diffraction pattern caused by the circular aperture of the telescope.

Apodizer: An apodizer is an optical element used in telescopes or imaging systems to modify the intensity distribution of light across the aperture. It can be used to reduce the intensity of diffraction patterns or to improve image contrast by altering the shape of the point spread function.

Attenuate: In astronomy, attenuate refers to the reduction in the intensity of radiation or light.

Cold start: In the context of planetary formation, a cold start refers to a scenario where a planet forms via gravitational collapse from a cold, dense cloud of gas and dust without undergoing a phase of significant heating.

Hot start: In contrast to a cold start, a hot start in planetary formation refers to a scenario where a planet forms through rapid accretion of material often involving significant heating processes.

Inner Working Angle (IWA): In astronomical observations, the inner working angle refers to the separation where the peak flux of the star is attenuated by 50%.

2 Direct imaging of exoplanets

Lyot stop: A Lyot stop is a specialized aperture stop used in certain types of coronagraphs to block the light of the central star, particularly stray light and diffraction artifacts, while allowing the light from the target object to pass through. It helps to improve the contrast of faint objects near bright sources.

Occluding Mask: An occluding mask is a device used in telescopes or coronagraphs to block or mask out the light from a central bright source, such as a star, allowing fainter objects nearby, such as exoplanets or protoplanetary disks, to be observed more easily.

Outer Working Angle (OWA): Similar to the Inner Working Angle (IWA), the outer working angle refers to the maximum angular separation at which the adaptive optic of the system is performing.

Point Spread Function (PSF): The point spread function describes the response of an imaging system, such as a telescope or camera, to a point source of light. It characterizes how the light from a single point in the object is spread out in the resulting image.

Post-processing: Post-processing in astronomy refers to the digital manipulation and enhancement of images or data obtained from telescopes or other observation instruments after they have been initially captured. This can involve techniques such as noise reduction, image stacking, and enhancement of specific features.

Snow line: Also known as the frost line or ice line, the snow line is the distance from a central star at which the temperature in a protoplanetary disk drops low enough for volatile compounds like water, methane, and ammonia to condense into solid ice grains, affecting the composition of forming planets.

Speckle: In astronomy, speckle refers to small-scale fluctuations in brightness or intensity observed in images of celestial objects caused by atmospheric turbulence or imperfections in optical systems.

Strehl Ratio: The Strehl ratio is a measure of the quality of an optical system, such as a telescope or camera. It compares the peak intensity of the point spread function (PSF) of the system to the ideal PSF for a perfect optical system. A higher Strehl ratio indicates better image quality and reduced aberrations.

Transitional Disk: In astronomy, a transitional disk refers to a type of protoplanetary disk surrounding a young star that exhibits a gap or inner hole in its dust and gas distribution. These disks are believed to be in a transitional phase of planetary formation, possibly indicating the presence of newly forming planets that have cleared material from their orbits.

Warm start: A warm start, similar to a hot start, describes a scenario in planetary formation where a planet forms through the rapid accretion of material onto a pre-existing core, but without undergoing as much heating as in a typical hot start scenario. This can result in different planetary compositions and structures.

Abstract

Over the past four decades, the exploration of planets beyond our solar system has yielded the discovery of over 5600 exoplanets orbiting different stars. Continuous advancements in instrumentation and cutting-edge techniques empower astronomers to unveil and characterize new exoworlds with increasing frequency. Notably, direct imaging, also called high-contrast imaging, stands out as the only method capable of capturing photons emitted directly from the planetary bodies.

This innovative technique proves particularly advantageous for scrutinizing nascent planetary systems, where planets shine brilliantly and emit significant heat during their initial developmental phases. Direct imaging provides comprehensive visuals of the entire system, encompassing the central star, potential circumstellar disks, and any additional companions.

However, the complexity of imaging an object millions of times fainter than its parent star necessitates state-of-the-art instrumentation. High-contrast imaging demands cutting-edge tools such as extreme adaptive optics systems, telescopes exceeding 8 meters in diameter, coronagraphs, and modern imagers. The pivotal role of post-processing cannot be overstated in the quest for detecting and characterizing planets through direct imaging. Substantial progress has been made in this realm since the first detection in 2005.

This method has not only facilitated the discovery of numerous planets but has also presented invaluable opportunities to explore the properties of young substellar companions, both planets and brown dwarfs. Insights into their interactions with parent disks or other companions within the system, the composition of their atmospheres, and the identification of still accreting planets, also known as "protoplanets," contribute significantly to our understanding of planet formation scenarios. The continued refinement of direct imaging techniques promises to unveil further revelations in the captivating field of exoplanetary exploration.

1 Objectives

- Learn the differences between the exoplanet detection techniques;
- Understand the effects of the atmosphere on the observations;
- Learn about the instrumentation needed to perform high-contrast imaging;
- Know the possible post-processing techniques of the high-contrast imaging;
- Investigate the history of the direct imaging technique and some of the benchmark results;
- Learn about the different theories of planet formation;
- Understand what are the protoplanets, and why we are so interested in them;
- Discern the different types of sub-stellar objects.

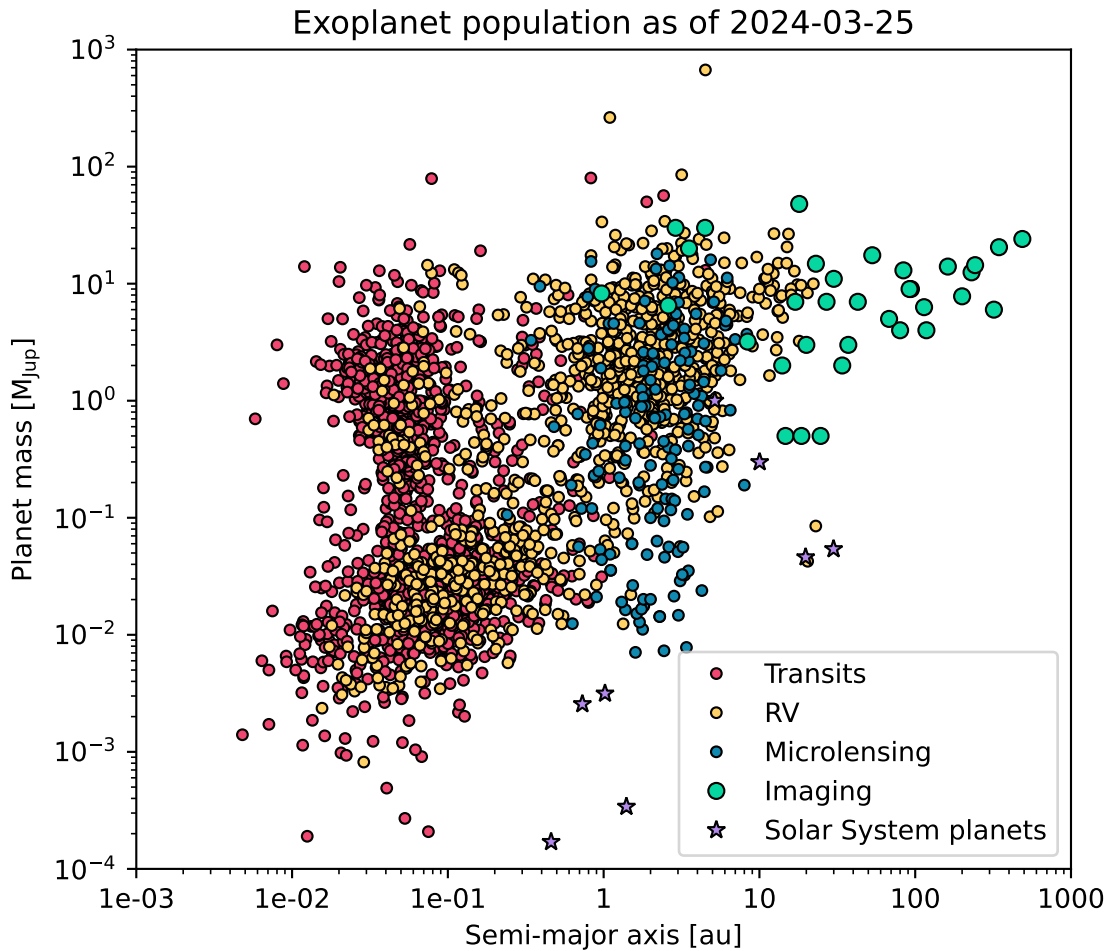


Fig. 1 Exoplanet population in the mass (in Jupiter masses) vs separation (in au) diagram. Each technique is represented with a different color and populates a different region of the diagram. Direct imaging detects planets at wide separations, exploring the outer part of planetary systems.

2 Introduction

In our Galaxy, as of February 2024, there are currently ~ 5600 known exoplanets, which are planets orbiting stars other than the Sun¹. Different detection techniques have contributed to the diverse sample of exoplanets, each focusing on specific types of objects. Transits, the slight dimming of a star's light as an exoplanet passes in front of it from our point of view, reveal planets in close proximity to their parent stars and account for the majority of current detections, spanning a wide range of masses. Radial velocities, the wobble in a star's motion caused by the gravitational pull of an orbiting planet, favor short separations and can detect low-mass planets. On the other hand, gravitational microlensing, the brief brightening of a distant star due to the gravitational field of a foreground star-planet system acting as a magnifying lens, is sensitive to planets at intermediate separations but lacks follow-up observations. Additionally, astrometry, the measuring of tiny shifts in a star's position caused by the gravitational pull of an orbiting planet, can detect massive planets at intermediate separations. Figure 1 illustrates the mass vs separation diagram, displaying the current exoplanet population.

In addition to these techniques, direct imaging, also called high-contrast imaging (HCI) stands out as the only method capable of directly observing giant gaseous exoplanets at wide separations, particularly in young systems (less than 500 Myr). Indirect techniques, in contrast, are influenced by stellar activity and primarily target older systems.

Direct imaging is the only technique exploring the outer part of planetary systems (Fig. 1), and the one that gives insights into giant planets still forming or recently formed. This technique started to detect planetary mass companions in 2005, and since then it has detected over 30 planets and several brown-dwarf companions. Even if the number of detections is significantly lower than other indirect techniques, direct imaging has several advantages that make every detection key to better understanding planet formation and dynamics of planetary

¹<https://exoplanet.eu/catalog/>

4 Direct imaging of exoplanets

systems.

Direct imaging consists of masking the light of the host star with a coronagraph or a nulling technique to reveal what there is around it. It is a challenging technique, as the contrast, i.e. the brightness ratio between the planet and its host star, is of the order of 10^{-6} even in rather favorable cases. For comparison, it is similar to detect a coin of the size of a dime close to a lighthouse, at a distance of 1 km. Also, the residual light of the star is brighter than the object of interest. The residual light is also called “the speckle pattern”, produced by the imperfections of the optical elements that scatter the light of the central star, it resembles a halo of thousands of bright point-spread functions. Advanced extreme adaptive optics (AO) instrumentation, coupled with coronagraphy and state-of-the-art imagers, are crucial to attenuate the speckle pattern and reveal planets detected through direct imaging, as presented in details in Sec. 3.

To detect faint companions, buried under the speckle pattern, and sometimes very close to the central star, the post-processing phase is key. The post-processing methods are intrinsically connected to the observing technique. The most common techniques optimized to detect and characterize companions are spectral differential imaging (SDI), angular differential imaging (ADI), and reference differential imaging (RDI). Those post-processing techniques are presented in Sec. 4.

Because of the complexity of the method, the number of the systems with confirmed HCI companions is significantly lower than the other indirect methods. The most emblematic direct imaging systems observed and studied so far are presented in Sec. 5. Some benchmark systems are described in more detail in the dedicated subsections. Every system directly detected is unique and provides insights into the formation scenario, the dynamics of the planet(s) in the system, the disk-to-planet interaction, and the composition of the atmosphere of the companion itself.

This powerful technique focuses on very young systems, as during the first stages of planet formation the entropy is high and planets are hot, self-luminous, and still very bright. Direct imaging is the only technique able to spatially separate the photons of young planets and it permits the measurement of their spectra. The technique uniquely paints a picture of the planetary system just after its birth, giving clues to the study of planet formation mechanisms (presented in Sec. 6).

Planets that are still forming, also known as “protoplanets” have been imaged with high-contrast imaging. Those objects are still undergoing mass accretion and they are an invaluable insight to understand where and how planets form. I present the known protoplanets and the challenging hunt for this kind of object in Sec. 7.

The objects of interest of the high-contrast imaging technique are not only planets but in general all sub-stellar objects, including brown dwarf companions. I present the different spectra of the objects of interest of the direct imaging technique in Sec. 8. The conclusions of this chapter and the future prospects of the direct imaging technique are presented in Sec. 9.

3 Instrumentation

The principles of adaptive optics are to attenuate the influence of the atmosphere by measuring its behavior at a high-frequency rate and correcting for its contribution quasi-simultaneously. The light of the stars, which by approximation comes from an infinite distance, should be a perfect plane wave when entering the pupil of the telescope. Following the law of the diffraction by a circular aperture, the angular resolution of a telescope with an aperture size D is defined as:

$$\theta_{\text{diff}} = 1.22 \frac{\lambda}{D}, \quad (1)$$

where λ is the wavelength of the observation. θ_{diff} is the radius of the inner Airy disk, of the order of 30 mas for $\lambda = 1 \mu\text{m}$ and $D \sim 8$ m. What is observed on the focal plane of a telescope is essentially the Fourier transform of the wavefront impinging on the pupil plane multiplied by the pupil shape (Fraunhofer approximation: see, e.g., Oppenheimer and Hinkley, 2009). The intensity of the Airy function is mostly concentrated in the first peak, inside θ_{diff} , then has secondary rings separated by minima of the function, with decreasing energy.

For ground-based telescopes, the light from the stars passes through the Earth’s atmosphere. This latter is formed by layers of turbulent “bubbles”, of size r_0 (Fried parameter), within which the wavefront remains coherent. The bubbles have different refraction coefficients so that the wavefront is corrugated before entering the pupil of the telescope. The variation of the refraction index is larger (causing larger deviations of the beam) at shorter wavelengths. For this reason, the wavefront error (measured in units of the wavelength) is larger at shorter wavelengths.

These bubbles act as subpupils of aperture r_0 which form point spread functions (PSFs) with dimension $\theta_{\text{atm}} = 1.22 \frac{\lambda}{r_0}$. Having two bubbles at a distance among each other $\sim D$ constitutes a two-beam interferometer which creates a pattern of linear interference fringes (Racine et al., 1999). Before the pupil telescope, there are sub-apertures of size r_0 and their fringes interfere constructively: these fringes constitute the variable “speckle pattern”. The speckles have a size of $\sim \lambda/D$, for the distance of the two sources of interference. The speckles have the same dimension as the PSF of the star so it is impossible to distinguish them from a real source of the same brightness.

To try to minimize this variable speckle noise, the AO uses a deformable mirror (DM) which permits to correct quasi-instantaneously the wavefront corrupted by the atmosphere. The wavefront sensor measures the wavefront corrugations, then a real-time control system calculates the correction to be sent to the DM, which has actuators that deform its shape. In order to model the atmospheric behavior, a point source, typically a star, is taken as a reference source. It has to be bright enough to permit a high signal-to-noise ratio (SNR) in the wavefront sensor. Some instruments have the possibility of using an artificial reference in addition to natural point sources, the laser guide star, when a bright star is lacking. Currently, most of the direct imaging instruments use the target host star itself as a reference for the AO.

To commensurate the goodness of the AO, a parameter defined as Strehl Ratio (SR) is used. It defines the ratio between the peak of the PSF measured in the detector and the theoretical diffraction-limited PSF. In Fig.2 the differences between the performance with

and without the AO are shown. A perfectly flat wavefront corresponds to the theoretical diffraction limit and then has $SR = 100\%$. A corrugated wavefront has an $SR < 100\%$. The larger the wavefront error, the lower the SR; for this reason, the Strehl ratio is higher at longer wavelengths. Also, as the Airy pattern dimension increases as λ , and the image flux is being conserved, the higher SR (longer wavelength) PSF has a brighter Airy pattern (core and inner rings) and a correspondingly lower intensity in its halo (Marois et al., 2000). While low-order AO can achieve SR of 20 – 60%, in the 1-2 μm wavelength range, extreme AO (ExAO, with a high number of actuators) can reach more than 90% SR, almost a diffraction-limited PSF, in the same wavelengths (see, e.g., the VLT/SPHERE manual²). This improvement does not come for free, brighter stars are needed for the ExAO, as the wavefront must be more finely sampled. The ExAO provides a stabilized, quasi-diffraction limited beam, which is then centered in the coronagraph. To perform HCI the stability of the star PSF is key, to ensure that the host star is well centered and masked under the coronagraph during the whole exposure.

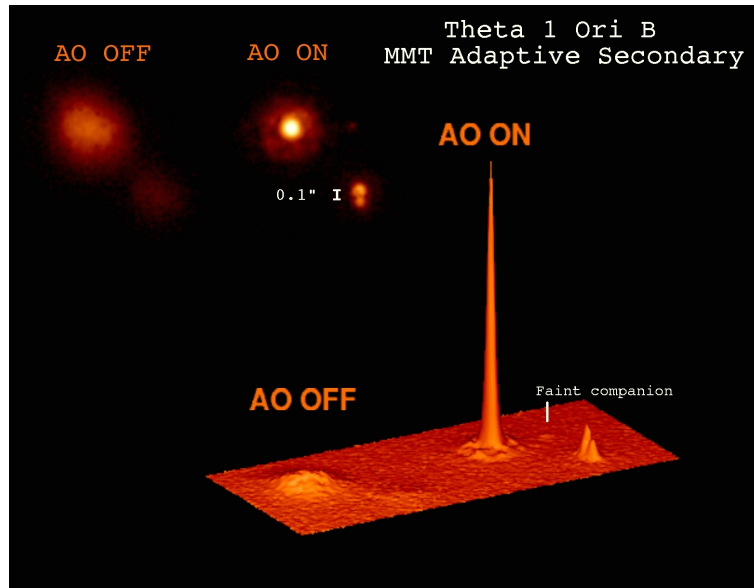


Fig. 2 Differences between the performance with and without the adaptive optics. In the upper-left corner, the system of θ^1 Orionis B is shown as seen in the detector of the instrument, with and without the AO. In the lower panel, the signal of the detector is shown in 3D, where the z-axis is the flux. Without the AO in the detector, two blurred blobs appear, when the AO is working, four objects are distinguishable. The SNR of each PSF increases when the AO is working. Credit: Laird Close, CAAO, Steward Observatory.

The AO can correct the wavefront errors up to a separation defined as the outer working angle (OWA). It is the angular distance corresponding to spatial frequencies above $N_{act}\lambda/2D$ where N_{act} is the number of actuators along a linear dimension of the DM and D the telescope aperture.

In addition to that due to the atmosphere, a second type of speckle pattern has to be taken into account: the quasi-static speckle pattern. The quasi-static speckles are due to the imperfections of the optics of the telescope, and they are mostly permanent during the exposure with typical lifetimes of tens of minutes (see e.g. Soummer et al., 2007). To attenuate this pattern, post-processing techniques are needed, as we will see in the next Section. The variable speckle pattern attenuated by the AO can be further suppressed during the post-processing by averaging the images during a long exposure.

The speckles are brighter going closer to the host star and this is a limitation for the direct imaging, as the majority of the planets detected are close to their host (see Fig. 1). In fact, the major limitations of the direct imaging technique are the faintness of the companion with respect to the host star and its small angular separation. The angular separation is defined as the projected on-sky separation of the companion with respect to its host star.

3.1 Coronagraphs

HCI exploits different kinds of coronagraphs to attenuate the light of the primary, which are divided into many types (see, e.g., Guyon et al., 2006). The main two categories are coronagraphs with occulting masks and phase masking coronagraphs. While the first class of coronagraphs uses an opaque mask that attenuates the first peak of the Airy function, the second class of coronagraphs exploits the principle of the destructive interference of the on-axis light.

²<https://www.eso.org/sci/facilities/paranal/instruments/sphere/doc.html>

One of the principal parameters of the coronagraph is the inner working angle (IWA) which is the radius where the peak flux of the star is attenuated by 50%. The goal of new coronagraphs is to decrease as much as possible this value, to be able to detect planets orbiting at small separations.

The most common types of coronagraphs used by high-contrast imaging instruments are:

- Apodized Lyot coronagraph (ALC): It is part of the first generation of coronagraphs. It includes three optical elements: the occulting mask in the focal plane stops the light within a short separation from the center (typically $\sim 0''.1$ in 8-10 m telescopes); an apodizer located on a pupil plane (in front of the focal plane) limits the diffraction of the light with a gradual transmission function. A Lyot stop after the focal plane attenuates the diffracted light by the mask in the focal plane. It then has a shape similar to the occulting mask of the pupil plane, as shown in Fig. 3 (also see, e.g., Guerri et al., 2009).
- Four quadrant phase-mask (4QPM): It is part of the second generation of coronagraphs. The mask (located in the focal plane) has a π phase shift in each quadrant. When the beam of light is centered there is destructive interference that suppresses the light. This type of coronagraph is reasonably achromatic (see, e.g., Rouan et al., 2000).
- Vector vortex coronagraph: It is part of the second generation of coronagraphs. The phase mask has different phases from 0 to 2π which creates destructive interference of the light (see, e.g., Mawet et al., 2009). The vortex coronagraph is particularly efficient in providing a deep contrast at a small IWA. Currently, it is used for wavelengths longer than $3 \mu\text{m}$ (L band mostly).
- Apodizing phase plate (APP) coronagraph: It is part of the last generation of coronagraphs. The APP is a type of pupil-plane coronagraph that works by modifying the complex field of the incoming wavefront by adjusting only the phase (see, e.g., Kenworthy et al., 2007). The advantage of this type of coronagraph is that the apodization is with phase only, which means that the throughput of the APP is higher compared to traditional amplitude apodizers. Its improved version, the vector-APP, is currently installed in 6 high-contrast imagers (Doelman et al., 2021). This version avoids chromatic biases and works in a wide wavelength range.

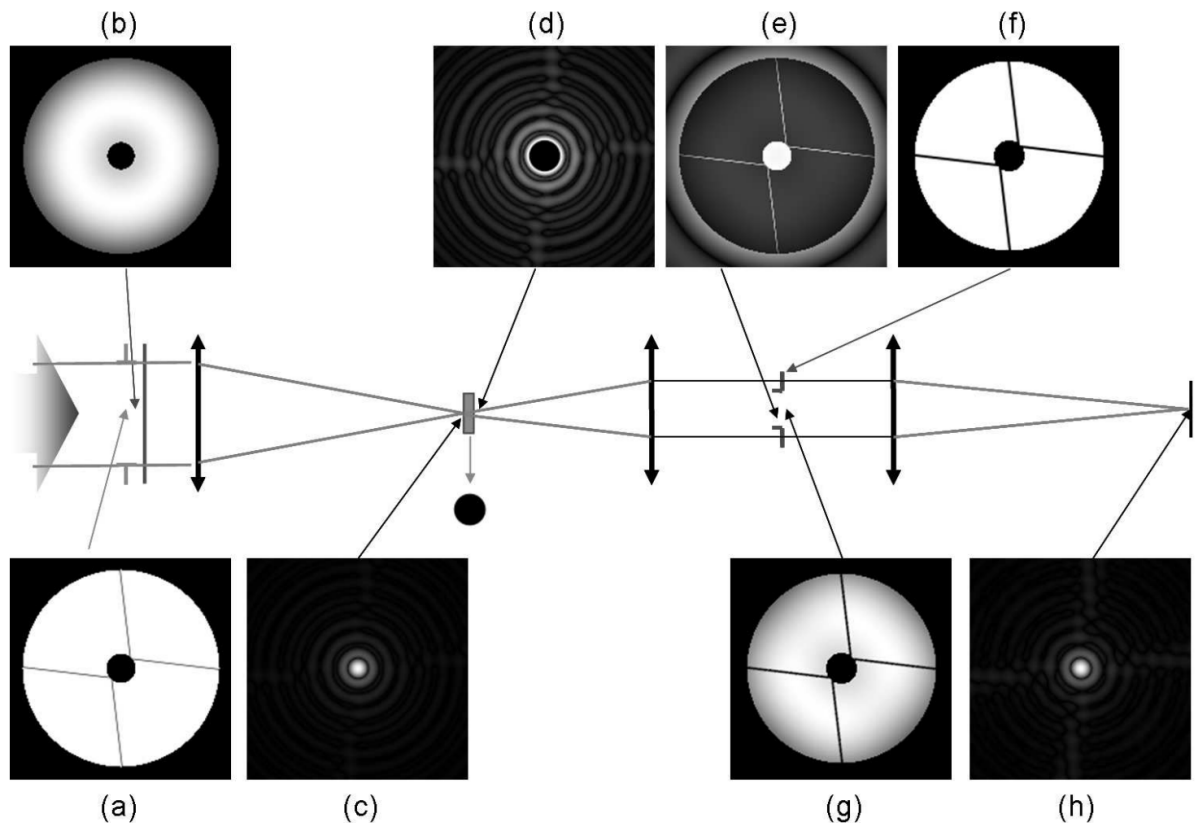


Fig. 3 Principles of the apodized Lyot coronagraph (ALC) with a VLT pupil. Light enters from the left and passes through the various stages as shown. (a) Entrance pupil, (b) Apodizer, (c) Point spread function (PSF) at the focus of the telescope, (d) PSF when the Lyot occulting coronagraphic mask is settled, (e) Pupil image before the Lyot stop introduction, (f) Lyot stop, (g) Pupil image with the Lyot stop, (h) Final coronagraphic PSF Image. Image and caption from Guerri et al. (2009).

4 Post-processing techniques

To attenuate the quasi-static speckle pattern various techniques can be applied, as presented in this Section. The techniques presented here are applied to detect and characterize exoplanets, on the other hand, there is another technique used to detect circumstellar disks, the Polarized Differential Imaging (PDI). I refer the reader to de Boer et al. (2020); van Holstein et al. (2020) and references therein for a detailed description of this method, as it is not presented in this Chapter.

4.1 The SDI technique

This technique exploits the fact that the speckle pattern, which is a diffraction pattern (as we saw in Sec. 3), scales with the wavelength, while planets remain in the same position independently from the wavelength, as they are real objects in the observed field. The spectral differential imaging (SDI, Racine et al., 1999) exploits this property to suppress the speckle pattern. The principle is to take simultaneously two coronagraphic images in two different bands with close wavelengths λ_0 and λ_1 . In this way, the speckle pattern is almost identical in the two filters. The image is rescaled at the longer wavelength λ_1 to have the speckles at the same position in both images with respect to the center of the detector. On the other hand, the planet is shifted from the original coordinates, according to the wavelength ratio, and has a different position in the two images. The two images (I) are then subtracted according to the formula:

$$I_{\text{diff}} = I_{\lambda_0} - k(I_{\lambda_1})_{\text{resc}}, \quad (2)$$

where k is a factor to correct for the flux amplitude of the speckle pattern, which can be different in the two filters. A cartoon of the SDI method is represented in Fig. 4.

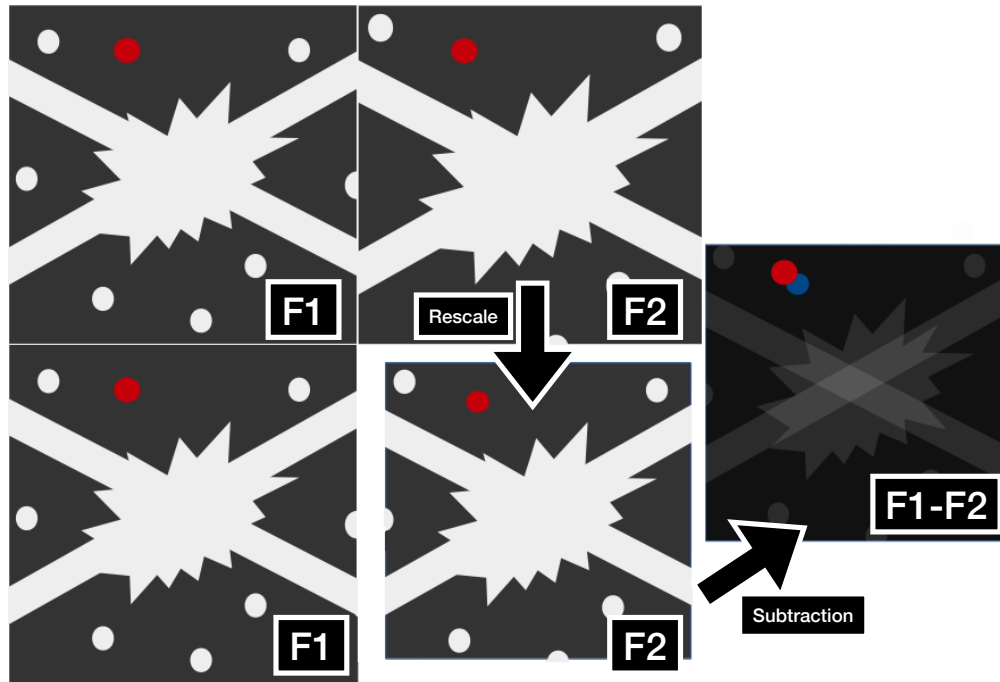


Fig. 4 How to combine images to exploit the SDI technique. The top-left image represents the raw frame of filter1 (F1) and the top-right filter2 (F2). In the second row filter1 is identical (lower left panel), while the image of filter2 has been rescaled to match the speckle pattern of filter1 (lower right panel). The product of the subtraction between the two filters after rescaling is shown on the right. The companion is represented in red, while its negative flux is represented in blue.

Also, this technique permits to distinguish a flat spectrum, where the fluxes are roughly the same in all the filters, from a spectrum that presents strong absorption in one of the channels, which will present different peak intensities in function of the wavelength. As we will see in Sec. 8, planetary spectra, especially T-type objects, present strong absorption in the bands of methane and water. For this reason, to observe in those bands, especially J and H , is convenient to distinguish a planet from a background star with a flat spectrum, as shown in Fig. 5.

The filter pairs of planet-finder imagers are specifically selected to be on- and off- the molecular lines of interest for exoplanets, not only the methane lines (in the near-infrared) but also, for example, the $H\alpha$ line in the visible to detect planets that are actively accreting (as we

will see in detail in Sec. 7).

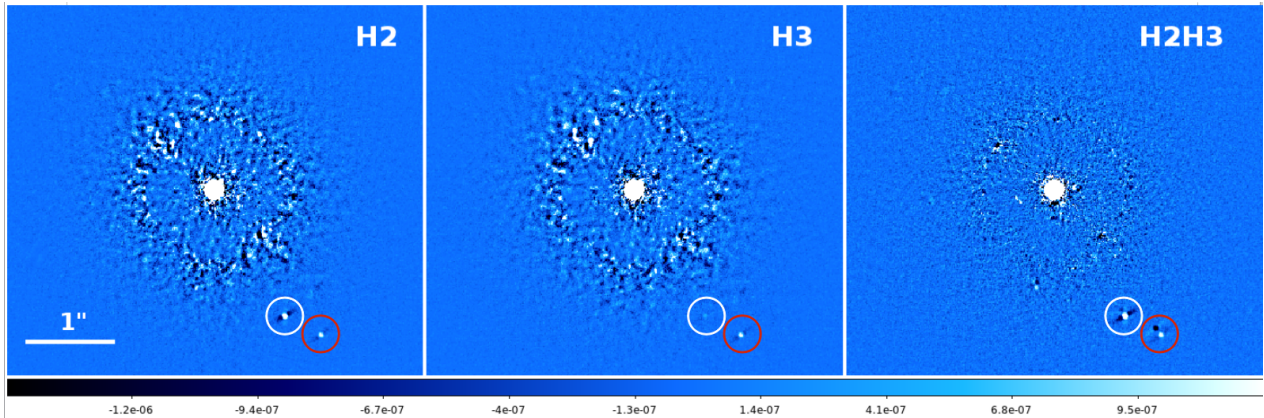


Fig. 5 Images of the system around GJ 758. The object in the white circle, GJ 758 B, is a late T-dwarf. In the red circle, a background star. The methane absorption in the $H3$ filter is evident, as the flux of the T-dwarf object is lower. In the SDI combination of the two filters, there is a clear difference between the T-dwarf and the background star close to it, the T-dwarf has a positive peak much brighter than the negative one, while for the star the two peaks are equally bright. Figure adapted from Vigan et al. (2016)

4.2 The ADI technique

Another fundamental observing method implied in HCI is the angular differential imaging (ADI; Marois et al., 2006). This technique uses the intrinsic field of view (FOV) rotation of altitude/azimuth telescopes to rotate the companions of the target around the center of the image, while the speckles remain as stable as possible during the observation (as we saw in Sec. 3). For an instrument at the Cassegrain focus³, the derotator of the telescope is switched off and the telescope pupil is fixed on the science camera. This observing setup is called “pupil-stabilized” mode. To exploit the maximum FOV rotation, the target is observed during the meridian passage, when the star is reaching its maximum altitude in the sky. The rotation rate ψ (in degrees per minute) of the FOV is calculated as:

$$\psi = 0.2506 \frac{\cos A \cos \phi}{\sin z}, \quad (3)$$

where A is the target azimuth, z the zenith distance and ϕ the telescope altitude (McLean, 1997).

In Fig. 6 the principle of a basic ADI is illustrated: the first step is to collect the images of the sequence, where the planet is slowly moving through the detector, while the speckles and the spiders are fixed (A_j); second, the images are combined with the median or other techniques to evaluate the speckles halo (B); then we subtract this product to the original images of the sequence (C_j); and derotate the images to have the planet at the same position (D_j) and the orientation with the North up and the East on the left; the result (E) is the combination of the derotated images.

The efficiency of this technique improves for greater angular rotation of the FOV during the exposure. It is widely used by every direct imaging instrument. ADI can be combined with SDI to reach a deeper contrast.

To post-process data from this observation technique there are many different reduction methods, among them I can cite:

- classical ADI (cADI; Marois et al., 2006): as explained above;
- smart ADI (sADI; Lagrange et al., 2010): a selection of the reference images which reconstructs the speckles halo is performed. While in the cADI all the images are taken into consideration and median-combined, in the sADI the closest-in-time frames to the reference image are excluded. This avoids the self-subtraction of the signal of the planet;
- radial ADI (rADI; Marois et al., 2006): it is a procedure similar to the sADI. This time the selection of the frames is optimized for the separation of the object, as the signal of the planet rotates along the frame at different angles as a function of the radius planet-center of the image. The PSF of the planet moves faster along the images for larger separations (i.e. we can reject fewer frames).
- Locally Optimized Combination of Images (LOCI; Lafrenière et al., 2007b): it is an algorithm that constructs an optimized reference image to subtract from a set of reference images. This image is built as a linear combination of the reference images selected, and the

³For an instrument at Nasmyth focus, the field rotates as the sum of the parallactic and altitude angle, while the pupil rotates as the altitude angle. A suitable optical element (e.g. a K-mirror) derotating the image as wished may then be located in front of the instrument, allowing stabilizing the image of the pupil on the detector; in this case, the field will rotate on the detector as the parallactic angle, as it is observed at the Cassegrain focus.

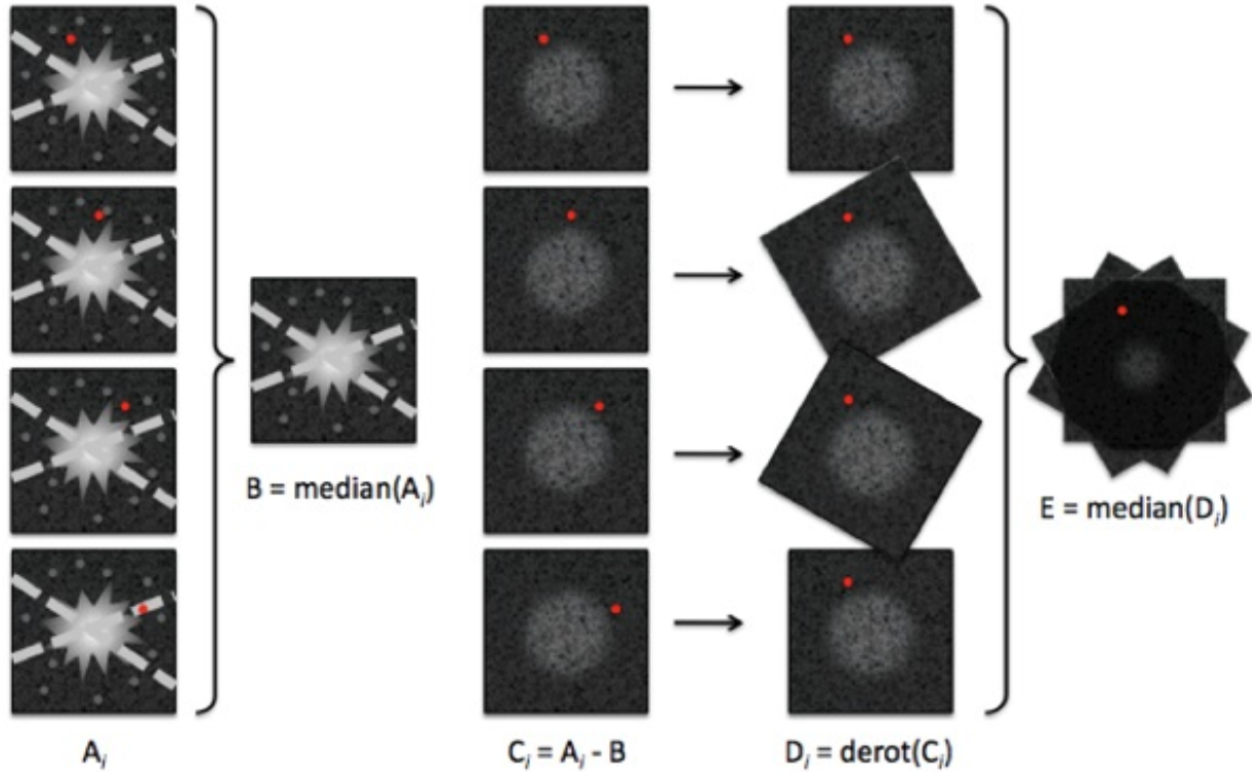


Fig. 6 Images combination to exploit the ADI technique. In the first column, the raw frames are displayed (A_i). In the second column, the median of the raw frames is shown (B). The third column shows the same raw frames A_i after the subtraction of the median of them (B). In the fourth column, each image has been derotated to have the North up and the East on the left (D_i). In the last column, the median E of the derotated frames (D_i) is displayed. The companion is represented in red. Credit: C. Thalmann.

coefficients of the combination are optimized inside multiple subsections of the image independently to minimize the residual noise within each subsection. There are also different flavors of LOCI, as for the ADI.

4.3 The RDI technique

The principle of Reference Differential Imaging (RDI) is that a model PSF of an isolated and disk-less reference star is taken and it is subtracted from the science frames. This technique is particularly useful for companions that are close to the host star (Xie et al., 2022). To fully take advantage of this method the “star-hopping” technique is being introduced, which consists of switching from the science target to the reference star multiple times during a sequence minimizing the observation overheads (see, e.g., Wahhaj et al., 2021). Since a very stable PSF is required to perform the RDI, space telescopes are the ideal instruments to successfully apply this technique.

5 Planetary systems detected with direct imaging

The direct imaging technique has been providing us with discoveries of sub-stellar companions for twenty years, when the first planetary-mass companion, 2MASS J1207334-393254 (2M1207 b, for simplicity) has been found with this method (Chauvin et al., 2005a). Today around 30 objects in the planetary mass regime, $M_p \lesssim 13 M_{\text{Jup}}$ (see Sec. 8), have been discovered with this method, but the number will increase rapidly with the new generation of high-contrast imagers mounted in space or on extremely large telescopes. The planetary-mass companions discovered so far are listed in Table 1. All of them orbit far from their host stars, spanning semi-major axes from $10 \lesssim a \lesssim 6500$ au. One of the goals of the current (and future) generation of instruments is to explore regions as close as possible to the host star. This means that shorter-period objects than the ones discovered so far will be probably detected in the near future. Also, the achievable contrast is increasing, unveiling perhaps other additional companions around the targets that we previously did not have the capability to detect. Among the direct imaging discoveries, only three multiple planetary systems have been discovered so far, composed of four planets around the star HR 8799 and two planets around both β Pictoris and PDS 70.

The results of HCI campaigns yield statistical results, even in the case of non-detection. For example, Biller et al. (2007) and Nielsen et al. (2008) found with 95% confidence level that less than 20% of stars have planets with a mass greater than $4 M_{\text{Jup}}$ between 20 and 100 au. Lafrenière et al. (2007a) estimated that less than 17% of stars have planets with a mass between 0.5 and $13 M_{\text{Jup}}$ on semi-major axes

Table 1 Planetary confirmed companions ($M \leq 13 M_{\text{Jup}}$) detected by the direct imaging technique. The distances to the systems are taken from Gaia collaboration et al. (2020).

Planet	M (M_{Jup})	a (au)	dist (pc)	Discovery paper
2M1207 b	5	42	65	Chauvin et al. (2005a)
AB Pic b	10–14	260	50	Chauvin et al. (2005b)
DH Tau b	11	330	134	Itoh et al. (2005)
HR 8799 b	~ 5	69.2	41	Marois et al. (2008)
HR 8799 c	~ 7	37.4	41	Marois et al. (2008)
HR 8799 d	~ 7	24.5	41	Marois et al. (2008)
1RXS 1609 b	8–14	330	145	Lafrenière et al. (2008)
β Pic b	9	10	19 ⁴	Lagrange et al. (2010)
HR 8799 e	~ 7	14.5	41	Marois et al. (2010)
2MJ0441+23 b	7.5	15	140	Todorov et al. (2010)
Ross 458 c	11	1168	11.7	Burgasser et al. (2010)
WD 0806-661 b	8	2500	19.2	Luhman et al. (2011)
HD 95086 b	~ 3	56	86	Rameau et al. (2013)
Gliese 504 b	4	43.5	18	Kuzuhara et al. (2013)
κ Andromedae b	13	100	50	Carson et al. (2013)
2MASS J0103 AB b	13	84	47	Delorme et al. (2013)
ROXs 42 (AB)b	9	140	135	Currie et al. (2014)
HD 106906 (AB)b	11	850	92	Bailey et al. (2014)
GU Piscium b	11	2000	48	Naud et al. (2014)
51 Eri b	3	11	29	Macintosh et al. (2015)
HIP 65426 b	7	87	109	Gratton et al. (2019)
2MASS J22362452+4751425	12	230	63	Bowler et al. (2017)
PDS 70 b	7	22	113	Keppler et al. (2018)
PDS 70 c	4	30	113	Haffert et al. (2019)
HD 169142 b	2	36	117	Gratton et al. (2019); Hammond et al. (2023)
2M0437 b	4	118	128	Gaidos et al. (2022)
YSES 2 b	6	114	109	Bohn et al. (2021)
COCONUTS-2 b	6.3	6471	11	Zhang et al. (2021)
AB Aurigae b	9–12	94	144	Currie et al. (2022)
AF Lep b	2–5.5	20.6	8	Mesa et al. (2023); De Rosa et al. (2023); Franson et al. (2023)
HIP 99770 b	13–16	16.9	41	Currie et al. (2023)

between 25 and 325 au, and at most 10% between 50 and 220 au. Chauvin et al. (2015) constrained the occurrence of planets more massive than $5 M_{\text{Jup}}$ to less than 15% between 100 and 300 au, and for companions more massive than $10 M_{\text{Jup}}$ to less than 10% between 50 and 300 au. From GPIES, Nielsen et al. (2019) found a clear correlation between the mass of the host star and the planet occurrence rate, with stars $> 1.5 M_{\odot}$ more likely to host giant planets ($5\text{--}13 M_{\text{Jup}}$) at wide separations (semimajor axes 10–100 au) than lower-mass stars. Around higher-mass stars, the total occurrence rate of such planets is 9%. Vigan et al. (2021) found that the frequencies of systems with at least one substellar companion with masses between 1 and $75 M_{\text{Jup}}$ and semimajor axes between 5 and 300 au are 23.0, 5.8, and 12.6% for BA, FGK, and M stars, respectively. The surveys mentioned above targeted hundreds of young and nearby stars, and among the planets discovered, some benchmark objects deserved particular attention and dedicated observations. In the following sections, I will present some of the well-studied systems discovered so far.

5.1 2M1207

2M1207 b is the first exoplanet detected with the direct imaging technique, it has been discovered using the instrument NACO, installed at the VLT (Chauvin et al., 2005a). The first epoch was obtained in 2004 when a promising object was detected around the star 2MASSW J1207334-393254 (Fig. 7), an M8 type star of the TW Hydra association (age ~ 8 Myr). The object is separated from the host star by about $0''.78$ ($= 55$ au). To confirm that the object is comoving, a second epoch was taken one year later, and the nature of the planet was confirmed. Following evolutionary models, a mass of $M = 5 \pm 2 M_{\text{Jup}}$ and an effective temperature of $T_{\text{eff}} = 1250 \pm 200$ K is found. It is considered more a binary system of low-mass objects, rather than a planetary system (Mohanty et al., 2007).

5.2 HR 8799

High-contrast observations with the Keck and Gemini telescopes have revealed in 2008 the first multi-planetary system ever imaged: four planets orbiting the star HR 8799 (Marois et al., 2008, 2010). One of the first images of the system is shown in Fig. 8. HR 8799 is a young

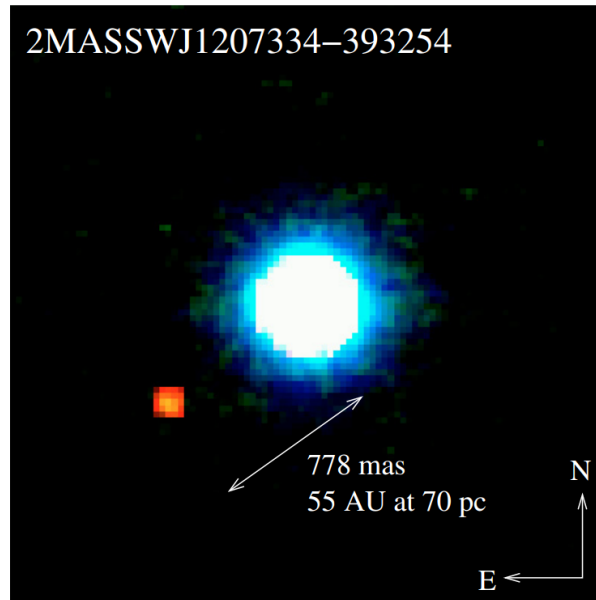


Fig. 7 The first planet ever detected with the high-contrast imaging technique: 2M1207 b (Chauvin et al., 2004).

star (~ 42 Myr), γ Doradus variable with λ Boo-like abundance patterns. The distance to the system is 40 pc (Gaia Collaboration, 2020).

This system is the most observed target with the direct imaging technique and a benchmark for the study of planetary atmospheres, dynamics of multi-planetary systems, and formation mechanisms. HR 8799 is particularly suited for this kind of observation since the contrast between the planets and the central star is favorable. The planets are also orbiting on a wide separation from the host star, making direct imaging observation relatively easy for most of the current high-contrast instruments.

For this reason, the planets around HR 8799 have been observed by different telescopes and instruments, providing a rich archive of astrometrical, photometrical, and spectroscopical information, invaluable to studying young planetary systems.

Astrometric follow-ups of the planets lasted two decades, permitting monitoring of the orbits of the 4 planets. In Zurlo et al. (2022) a detailed dynamical and orbital analysis is presented. The parameters for the 4 orbits are calculated assuming coplanarity, relatively small eccentricities, and periods very close to the 2:1 resonance. The dynamical masses for the planets have been estimated to be $8\text{--}9 M_{\text{Jup}}$ for the inner planets HR 8799edc, and $6 M_{\text{Jup}}$ for planet b. We refer the interested reader to these publications on the astrometrical characterization of the system: Sudol and Haghighipour (2012); Currie et al. (2012); Esposito et al. (2013); Maire et al. (2015); Pueyo et al. (2015); Zurlo et al. (2016); Konopacky et al. (2016); Wang et al. (2018); GRAVITY Collaboration et al. (2019).

Spectroscopy of the planets has been performed extensively and covers a wide wavelength range. The spectra recovered measure the emission of the planets themselves, without contamination from the host star. Among the results presented, I can cite Skemer et al. (2012); Marley et al. (2012); Oppenheimer et al. (2013); Ingraham et al. (2014); Greenbaum et al. (2018); Petit dit de la Roche et al. (2020); Ruffio et al. (2021); Wang et al. (2022). The variability of the atmospheres has also been monitored, although no evident signal of variability has been found (Apai et al., 2016; Biller et al., 2021)

5.3 Fomalhaut

Kalas et al. (2008) discovered the lowest mass planet ever imaged, Fomalhaut b (Fig. 9). This object has been imaged in visible light using Hubble Space Telescope (HST) Advanced Camera for Surveys (ACS), and it appears in the dust belt surrounding the brightest star of the constellation Piscis Austrinus. Fomalhaut is an A4 type star, 7.7 pc away, aged ~ 400 Myr. The planet is not detected in IR light. Neither Keck (L' band) nor Gemini (H band) have been able to detect it. This can suggest that the planet is (a) low mass and (b) detected in the visible through reflected light more than thermal emission. Its presence was predicted by the unusual sculpturing of the disk, which is highly inclined and off-centered. The origin of the planet is accepted to be in the debris disk, as it is still surrounded by it. Dynamical studies put an upper limit for the mass of the object of $3 M_{\text{Jup}}$. Fomalhaut b is on a very eccentric (0.8) orbit, with a semi-major axis of 177 au (Kalas et al., 2013). It should be mentioned that the nature of this object is still under debate, with the alternative that the object is instead a dust clump (see, e.g., Galicher et al., 2013; Kalas et al., 2013). Lately Neuhäuser et al. (2015) proposed that the companion is, in reality, a background neutron star, confirmed by Kennedy et al. (2023).

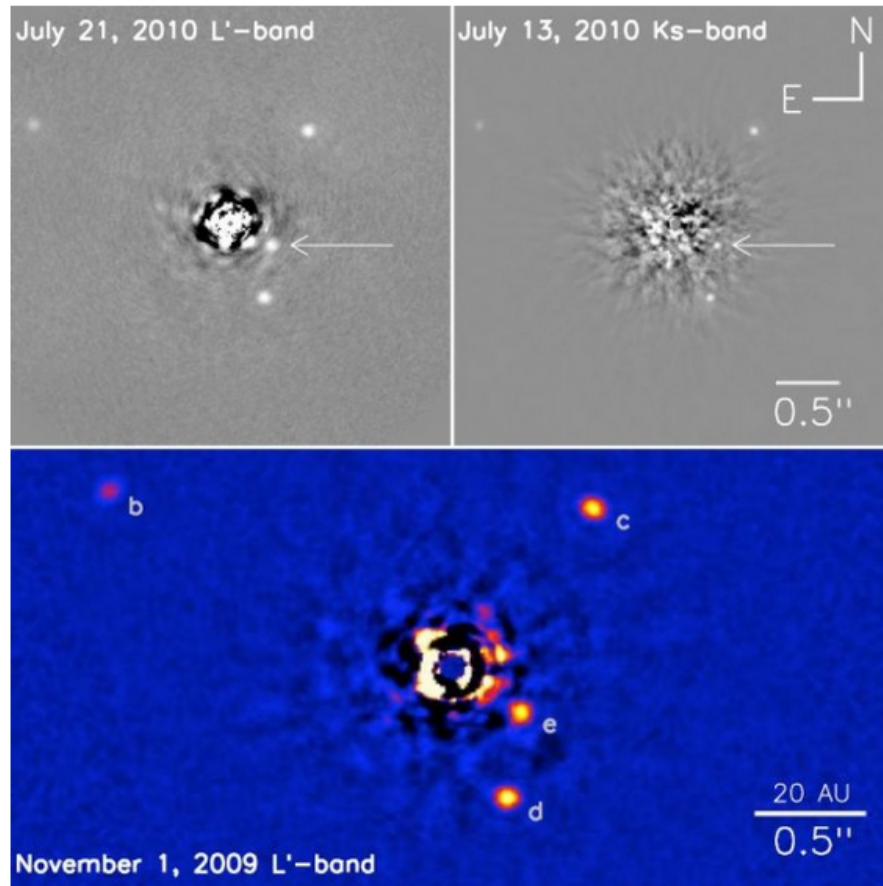


Fig. 8 The first multi-planetary system ever imaged: HR 8799 bcde (from Marois et al., 2010).

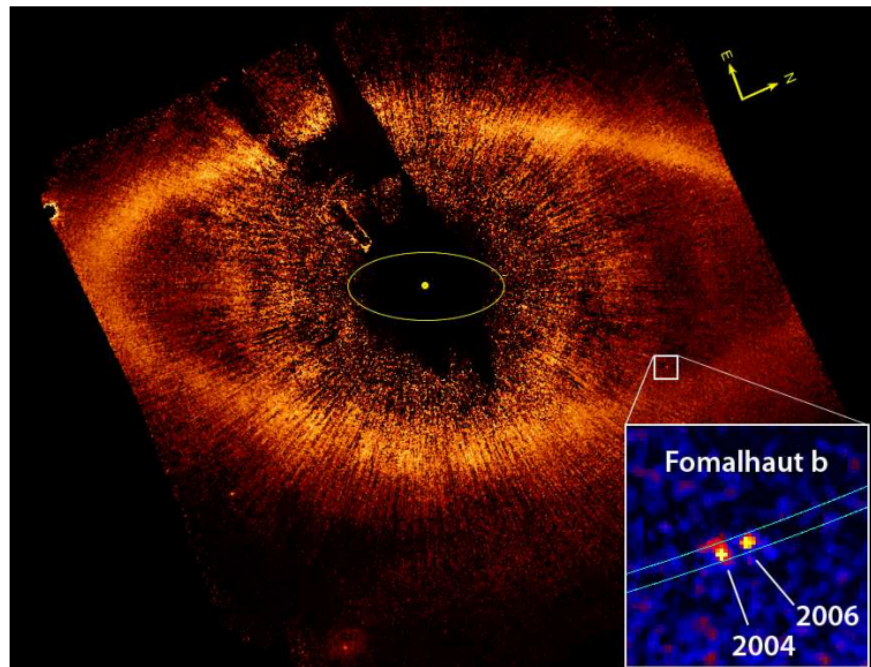


Fig. 9 Image of the debris disk surrounding the star Fomalhaut. The putative planet Fomalhaut b is seen in two different epochs (Kalas et al., 2008).

5.4 β Pictoris

Around the star β Pictoris, a planet has been discovered by Lagrange et al. (2009). The system also hosts an edge-on debris disk, as shown in Fig. 10. This planet has the closest semi-major axis for a direct imaging planet, 8 – 10 au, that corresponds to the snow line of the system, as the primary is an A-type star. As for the Fomalhaut planetary system, upper limits on the mass of the companion can be calculated from dynamical constraints. The mass of β Pic b has been estimated of $\sim 8 M_{\text{Jup}}$. The age of the system is assumed to be 18 Myr, as in Miret-Roig et al. (2020). The small projected separation of the system, $0''.4$, is no longer an issue for the new generation instruments, which are finally able to extract the spectrum of the companion (see, e.g., GRAVITY Collaboration et al., 2020).

β Pic turned out to be a multi-planetary system, with the radial velocity technique, a second companion was discovered (Lagrange et al., 2019). It orbits closer to the star, with a semi-major axis of 2.7 au. The second companion to the system, β Pic c, was directly confirmed using the VLTI/GRAVITY instrument and presented in Nowak et al. (2020). β Pic c is the first planet discovered with the radial velocity technique and confirmed by direct detection. Having both information on the radial velocity and luminosity of the planet can constrain the dynamical mass of the object, and it is invaluable information to confirm the predictions of evolutionary models. Its mass is about $8 M_{\text{Jup}}$ (Lagrange et al., 2020).

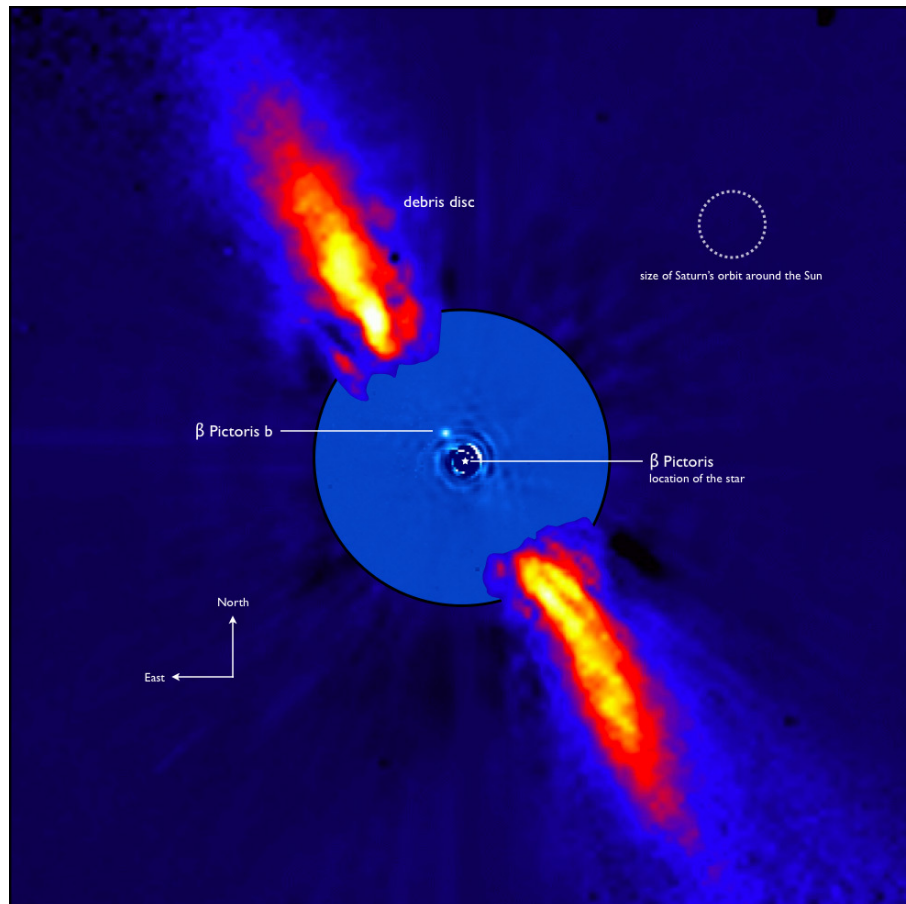


Fig. 10 Image of β Pic, showing planet b and the debris disk around it (Lagrange et al., 2009).

5.5 PDS 70

PDS 70 is one of the most emblematic systems discovered with the direct imaging technique. The host star is a K7-type member part of the Scorpius-Centaurus association (Pecaut and Mamajek, 2016). The distance to the system is 113.47 pc (Gaia Collaboration, 2020). The star is surrounded by a protoplanetary disk with a wide cavity. For the first time, a planet was discovered inside the gap of the disk, PDS 70 b (Fig. 11 and Keppler et al., 2018). For the discovery, the instruments SPHERE and NACO at the VLT were used. Given the young age of the system, 5.4 ± 1.0 Myr, the mass of the planet was estimated around $5\text{--}9 M_{\text{Jup}}$ (Keppler et al., 2018; Müller et al., 2018). Planet b was then imaged in the $H\alpha$ filter, demonstrating signs of accretion (Wagner et al., 2018, see also Sec. 7 on the implication of this discovery). A subsequent follow-up with the instrument MUSE revealed that the star hosts two planets, the other planet c was detected at

14 Direct imaging of exoplanets

a separation of 30 au, and both planets are actively accreting. This discovery was crucial as it provided direct observational evidence of ongoing planet formation in a protoplanetary disk. The planets that are still in the process of accreting material from the surrounding disk are called “protoplanets” (as we will see in Sec. 7).

The system was also imaged at longer wavelengths to study the disk properties (Isella et al., 2019). In 2021, a groundbreaking discovery was announced, adding even more focus to this emblematic system. At very high resolution, for the first time, a circumplanetary disk was detected around planet c (Fig. 12 and Benisty et al., 2021). Future follow-ups on the circumplanetary disk detected around planet c, or new detections around other companions, will provide information on the formation of satellites around giant planets.

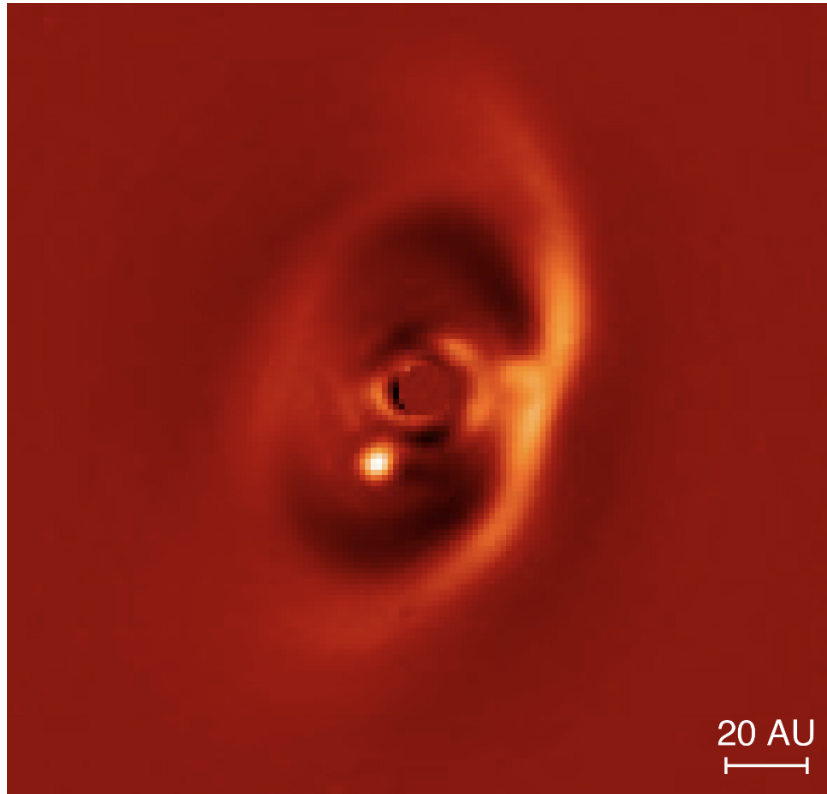


Fig. 11 Image of PDS 70, showing the first detection of planet b and the cavity of its protoplanetary disk (Keppler et al., 2018).

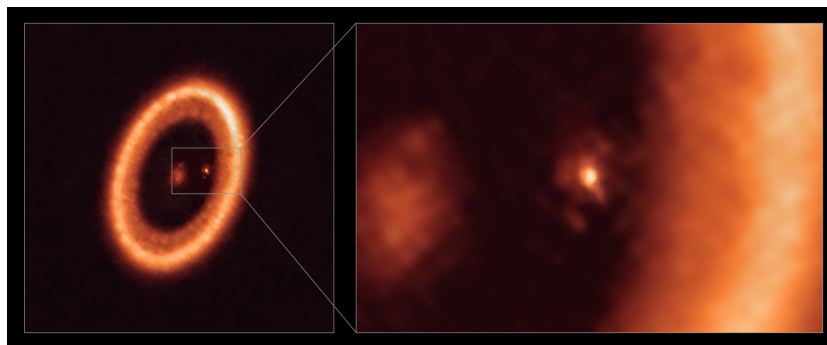


Fig. 12 Image of the circumplanetary disk around PDS 70, the first ever detected (Benisty et al., 2021).

5.6 AF Lep

AF Leporis is a star of the β Pic moving group. Very recently, three independent publications, Mesa et al. (2023); De Rosa et al. (2023); Franson et al. (2023) discovered a Jupiter-like planet around the star (Fig. 13). This is the third discovery in the same moving group after β Pic b and 51 Eri b. The age of the system is the same as the other stars in the moving group, around 20 Myr. The star was observed with high-contrast imaging for being an accelerating star. The presence of a companion was foreseen by comparing the astrometric values taken by Hipparcos and Gaia. The mass of the planet is estimated to be smaller than $5 M_{\text{Jup}}$, on an orbit of $a=21$ au. It is one of the lowest-mass planets detected with the direct imaging technique. Once again, combining the results from two different techniques, HCI and the Gaia-Hipparcos acceleration, provided stronger constraints on the mass determination of the companion.

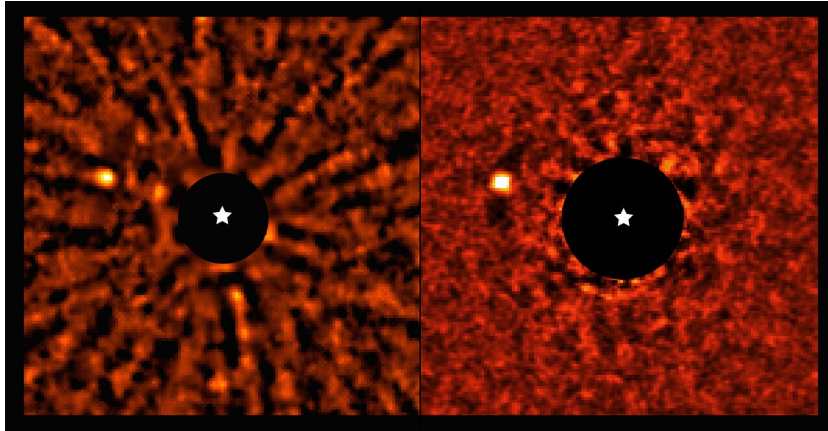


Fig. 13 The VLT/SPHERE detection of AF Lep b (Credit: ESO and Mesa et al., 2023; De Rosa et al., 2023).

6 Mechanisms of giant planet formation

Despite the wealth of exoplanets detected, numerous questions regarding planet formation remain unanswered, such as the processes and locations where planets originate. The two most widely accepted scenarios for planet formation are the *core accretion* (CA, Mizuno, 1980; Pollack et al., 1996) and the *gravitational instability* (GI, Cameron, 1978; Boss, 1997) models.

6.1 Core accretion model

One of the theories of planet formation most widely accepted is the so-called *core accretion* model (Mizuno, 1980; Pollack et al., 1996). It is the mechanism mostly accepted for the formation of giant gas planets in our solar system and in exoplanetary systems, at least for objects orbiting closer than 10-50 au (Perryman, 2014). This scenario is based on the fact that in the protoplanetary disk solid objects, called *planetesimals*, are present. These objects can collapse on a solid core, created from dust if located inside a zone where the protoplanet has gravitational influence. The solid cores can be formed more easily in the outer part of the disk, beyond the snow line, where the temperature is low enough for the formation of water ices. The feeding zone can extend over a few Hill radii $R_H = a(M_p/3M_\star)^{1/3}$, where a is the planet orbital radius, M_p and M_\star is the protoplanet and star mass respectively (Baraffe et al., 2010). When the solid core (ice and rock) has reached a mass of $\sim 0.1 M_\oplus$ it starts to gather an envelope of nebular gas. In this phase, there is a quasi-static balance between radiative loss and accretion energy. When the gas accretion has reached a critical mass M_{crit} a gravitational contraction occurs to compensate the radiative loss. The critical mass is reached when the mass of the core and the envelope are roughly equal (Mordasini et al., 2008). The critical mass can be estimated to be in the range 5-15 M_\oplus depending on physical conditions and assumptions about grain opacity (see, e.g. Pollack et al., 1996). When the critical mass is reached, the envelope can stay no longer in hydrostatic equilibrium. It begins to contract and the gas falls in free fall onto the core. The radius of the newborn planet is fixed by the conditions of this radiative shock. The accretion process terminates when the planetesimals and gas supplies end, as a gap in the disk may be created or because the disk gas dissipates at some point.

An example of a simulation of Solar system giant planets formation is given by Pollack et al. (1996). The process is divided into three phases: (i) the embryo of the protoplanet accumulates planetesimals in the first 5×10^5 yr, and there is a depletion of its feeding zone; (ii) the accretion rate remains constant during ~ 7 Myr, and the growth accelerates during the beginning of the phase (iii) with a runaway accumulation of gas. The results of these simulations are shown in Fig. 14. During the first years, the planet accumulates solids by rapid runaway accretion; this “phase 1” ends when the planet has severely depleted its feeding zone of planetesimals. The accretion rates of gas and solids are nearly constant during most of the duration of the phase 2. The planet’s growth accelerates toward the end of phase 2, and runaway accumulation of gas characterizes the phase 3. The simulation was stopped when accretion became so rapid that the model

broke down. The endpoint was thus an artifact of the technique. As expected, the final mass of the planet is proportional to the density of planetesimals of the feeding zone, even if the core is initially of the same dimension. The core of Jupiter predicted by these simulations is more massive than the current estimation. This is one of the issues which has to be explained by the core accretion models.

The major problem of this theory is that the protoplanetary disk lifetime, few Myr, is shorter than the time needed for a core to grow. The growth timescale is proportional to $a^{3/2} M_{\star}^{-1/2}$, for that planets far away from the host star cannot be formed there (D'Angelo et al., 2011). To solve this issue, Hourigan and Ward (1984) first proposed the mechanism of migration. In this way, planets can move from their formation position. Migration occurs when the torques exerted by the different parts of the disk interact with the planet. It reacts by adjusting its semi-major axis to compensate for the forces. There are primarily two types of migration: type I, the migration of low mass planets (see Goldreich and Tremaine, 1980; Tanaka et al., 2002), and type II, where massive planets open a gap in the protoplanetary disk and migrate (Lin and Papaloizou, 1986). This mechanism permits the core to accrete on different zones where it can find new planetesimals as the lengthy phase II is skipped (Alibert et al., 2004).

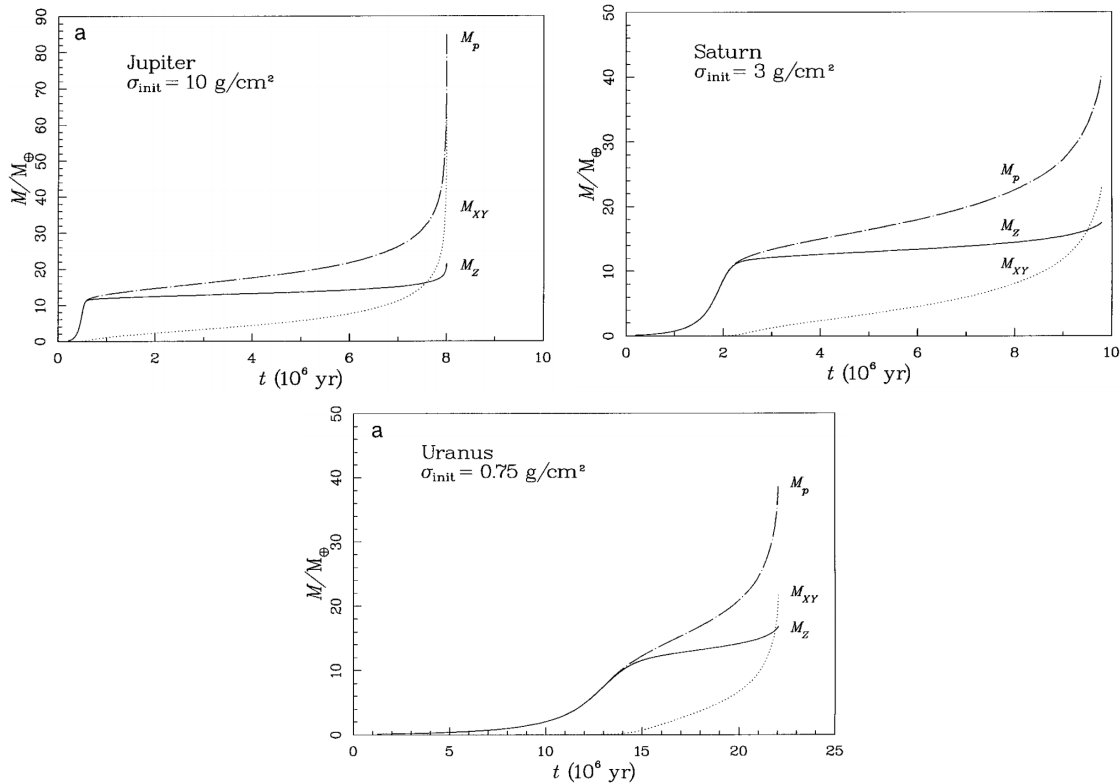


Fig. 14 Figures 1, 4, and 5 from Pollack et al. (1996). Results on the simulations performed on the formation of the solar system giant planets. The initial planetesimal surface density, σ_{init} is shown for each planet. The initial embryo has nearly the mass of Mars, and planetesimals have a radius of 100 km. The solid line (M_Z) represents accumulated solid mass, the dotted line (M_{XY}) accumulated gas mass, and the dot-dashed line (M_p) the planet's total mass.

The Solar system can be at the same time good evidence for the core accretion model and against it. The outer Solar system is consistent with the trend of time scale/radius. The less massive planets could have been formed during the beginning of the dissipation of the gas. Also, Jupiter has the closest Solar composition, while the other giant planets are poorer in gas (Armitage, 2007).

Against the model, there is the difficult explanation of the Neptune time scale. To avoid this problem, migration of the planet is proposed. Also problematic is to explain the small core of Jupiter, as we saw before, even if a core erosion may have occurred.

Concerning exoplanets, the correlation between the frequency of planets and the metallicity of the host seems to confirm the core accretion scenario, as it is more probable to form planets faster around high metallicity stars. On the other hand, one should consider that this statistical analysis is biased by the high number of close-in planets discovered so far, and it could be different for long-period planets.

To avoid the problems raised by the core accretion model and to explain exceptions found in the exoplanet population, especially for objects at great distances from the host, another scenario has been proposed, presented in the next Section.

6.2 Gravitational instability

An alternative theory to the core-accretion model suggested especially to obviate the timescale problem, is the *gravitational instability* scenario (Cameron, 1978; Boss, 1997). Following this theory it is possible to explain the formation of massive planets, far from their host star. A condition for this scenario is that the disk is massive. Instability perturbations may occur in a disk if the Toomre stability condition falls:

$$Q = \frac{c_s \kappa_e}{\pi G \Sigma} \sim \frac{M_{star} H}{M_d r} < 1 \quad (4)$$

where c_s is the speed of sound, κ_e is the epicyclic frequency in one point of the disk, $\Sigma \sim M_d/r^2$ is the surface density, H is the disk vertical scale height and M_d is the mass of the disk within the radius r (Toomre, 1964). If this occurs, the disk fragments into pieces, and from the clumps that they cause, future giant gas planets can form.

A steady-state disk becomes less stable at large radii (Armitage, 2007). If the mass accretion rate increases, the radius decreases. Examples of simulations by Boley (2009), performed to predict the formation of planets by gravitational instability are shown in Fig. 15. Three out of four synthetic disks present clumps at the end of the simulation.

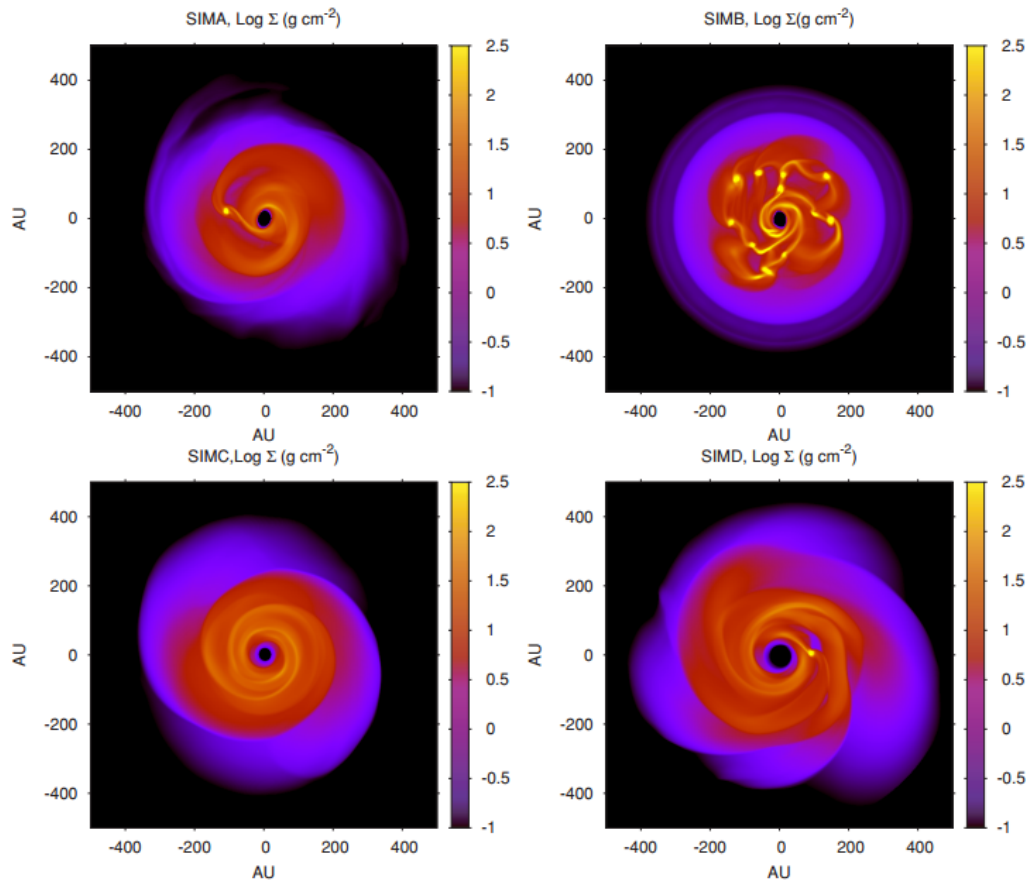


Fig. 15 Figure taken from Boley (2009). Snapshots of the surface density of the disk at the end of different simulations to predict gravitation instability formation. In three out of four cases, the gravitational instability bursts lead to fragmentation and formation of clumps.

Another parameter that plays an important role is the temperature of the disk. Lower-temperature disks may be more likely to be unstable. This mechanism is faster than the core-accretion one, taking less than 1 Myr. This is due to the fact that disk fragmentation is possible if the cooling time is shorter than the orbital period.

The first-time evidence of a spiral arm of a disk fragmenting into planet-forming clumps was found around the FUor star V960 Mon (Weber et al., 2023). Comparing scattered light images of the massive disk around the star with SPHERE and ALMA data they discovered that unresolved clumps are detected in the sub-mm at the same location of the spiral arm seen in scattered light (see Fig. 16).

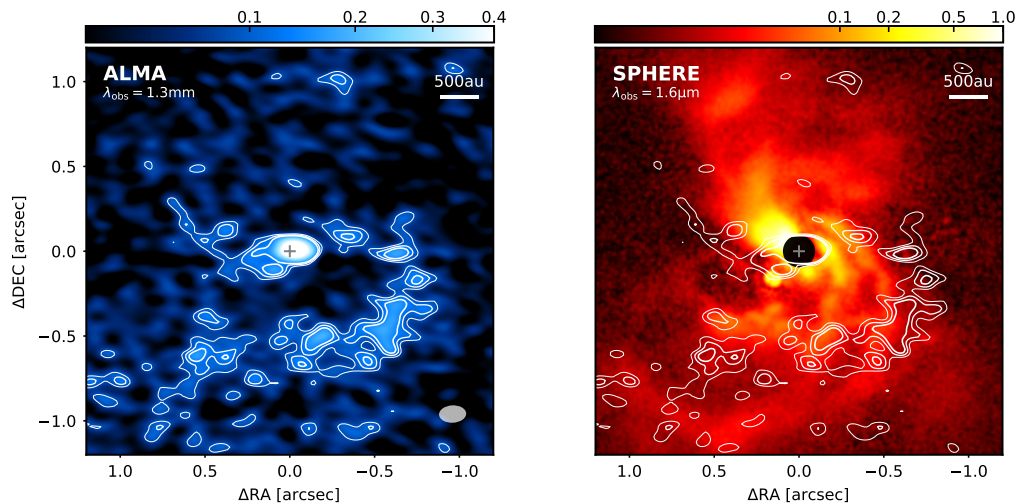


Fig. 16 First evidence of gravitational instability clumps with planetary masses. On the left, the ALMA band 6 continuum image of the protoplanetary disk around the FUor star V960 Mon, and on the right the SPHERE/IRDIS polarized light image. Contours of the ALMA continuum are overlaid on both images, corresponding to levels of 3, 4, and 5 times σ . The ALMA signal showing the clumps share the same location of the spiral arms around the star. Image from Weber et al. (2023).

This is the first direct detection of gravitational instability clumps in the planetary-mass regime. This direct detection of clumps within a protoplanetary disk represents an unprecedented achievement in the field. Studying FUor objects and their connection to gravitational instability is critical not only for understanding episodic accretion processes but also for deciphering the formation of gas giant planets and the controversy between GI and CA scenarios. In recent years, the latter has been favored due to a lack of observational evidence supporting GI. At the moment of observation, the majority of protoplanetary environments do not meet the mass requirements necessary to initiate GI, and the ordered, smooth structures commonly found in Class II disks appear to contradict the occurrence of large-scale instabilities.

The planets formed by gravitational instability are expected to be far away from the host star and to have great planetary radii. Also, differently from the core accretion model, no core is expected. This model predicts that planets have a high initial entropy. For this reason, we define “hot-start” the birth of planets in the gravitational instability scenario, and “cold-start” the one of the core accretion. This is crucial when we want to assume a mass for planets during the first stages of their life, as the “hot-start” planets are much brighter for a fixed mass. On the other hand, Mordasini (2013) proposed that planets with massive cores, formed by core accretion, can also have high entropy during the first stages.

This scenario has been proposed to explain some of the directly imaged systems as HR 8799 (Marois et al., 2010), or planets around multiple systems (Kratzer et al., 2008, 2010a,b). Also, it could explain the fact that Jupiter has a smaller core than expected from core accretion. Finally, planets formed by core accretion have a limit on the mass, depending on the critical mass reached by the core. On the other hand, gravitation instability can explain massive planets formation. Boley (2009) proposed to unify these two theories that can coexist, by demonstrating that the core accretion can operate in the internal part of the disk (~ 100 au) while gravitational instability clumps can form planets in the outer region.

The direct imaging method will help us understand the formation of planets in wide orbits, which are not explored by the other indirect techniques. Also, measuring the luminosity of planets during the first stages of their life will help us understand which is the scenario that better describes the formation of each individual planetary system. Coupling the estimated mass from “hot-start” and “cold-start” models and dynamical information on the mass will be fundamental to comprehending how giant planets form.

7 Protoplanets

Understanding the formation of planets is of paramount importance in astrophysics, with implications for our understanding of the origin and diversity of planetary systems (see, e.g., Spiegel and Burrows, 2012). Previous breakthroughs in HCI have highlighted the potential of detecting protoplanets, or still forming planets, through the $H\alpha$ emission, which serves as an indicator of accretion onto compact bodies (see, e.g., Rigliaco et al., 2012). Notable successes include the detection of a close stellar companion around HD142527 (Close et al., 2014; Claudi et al., 2019) and the strongest detection to date: two accreting protoplanets around the star PDS 70, which hosts a gapped protoplanetary disk (Keppler et al., 2018; Wagner et al., 2018; Haffert et al., 2019, and Fig. 17).

Approximately $\sim 30\%$ of Herbig Ae/Be disks should host giant planets of ~ 0.1 to $10 M_{\text{Jup}}$ (Kama et al., 2015), and should be classified as “transitional disks” (TDs), which are peculiar disks with cavities, gaps, and spiral structures that can be induced by the presence of such a

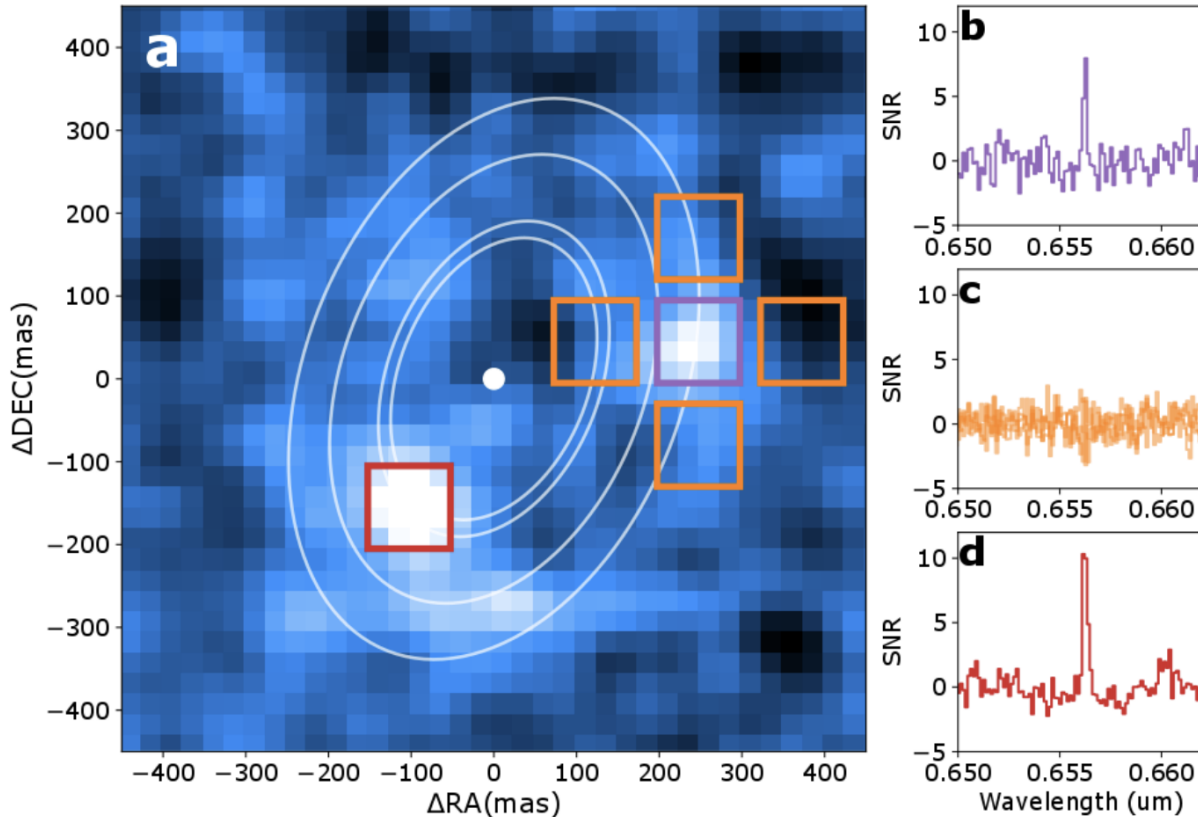


Fig. 17 Figure and caption taken from Haffert et al. (2019). Accreting protoplanets around the system of PDS 70. The $H\alpha$ detection map with an overlay of the contours of the orbital radii and a white dot in the center that marks the position of the star. The contours for PDS 70 c are the minimum and maximum orbital radii found for the different wavelength observations. For both objects the square apertures that were used for the photometry are shown, with the red aperture for PDS 70 b and the purple aperture for PDS 70 c. b, c, d, The corresponding spectra divided by their standard deviation are on the right and centered around the $H\alpha$ line position. The four apertures in orange indicate reference areas that are used to compare with PDS 70 c. The orange reference spectra on the right do not show any spectral feature, while both PDS 70 b and c clearly show $H\alpha$ in emission.

companion (e.g., Dodson-Robinson and Salyk, 2011; Stadler et al., 2023). Supporting this theory, hydrodynamical simulations predicted the presence of substellar companions around some observed TDs (e.g., Dong et al., 2015), but the putative objects have not been detected yet. Moreover, the planet's radiative feedback (i.e., intrinsic planet luminosity as a consequence of planet accretion) is an important ingredient that affects the evolution, morphology, and emission of the disk (Montesinos et al., 2015).

To confirm a protoplanet detection remains a difficult task, in fact in the past several candidates turned out to be disk features rather than forming planets. The first protoplanet candidate was announced in Sallum et al. (2015), around the young star LkCa 15. They found $H\alpha$ emission from a source close to the inner ring of the protoplanetary disk. The discovery was later on revisited by Thalmann et al. (2016), where the feature was presented as a portion of the disk. Other candidates are not confirmed, for example, the ones around the star HD 100546 (Quanz et al., 2013; Currie et al., 2015). Two planets have been detected, but following studies did not confirm their orbital motion and were not detected in $H\alpha$ (Rameau et al., 2017; Sissa et al., 2018).

An emblematic discovery is the protoplanet around AB Aur (Currie et al., 2022). The companion is located at a wide projected separation from the star (93 au) and it shows emission in $H\alpha$. The system shows spectacular spiral arms, an indicator of the presence of perturbing companions. Similarly, an embedded young planet has been found around the star MWC 758 (Wagner et al., 2023). This planet, at a projected separation of 100 au, is compatible with the shaping of the spiral arms around the system. No signal is recovered in $H\alpha$ at the location of the planet (Cugno et al., 2019; Zurlo et al., 2020).

Exploring the connection between the presence of (sub)-stellar companions and the structures observed in many protoplanetary disks, such as gaps, spirals, and rings, remains a significant challenge. The limited visibility of many newborn planets, still embedded in their disks and entangled with scattered light from the circumstellar environment, could explain the absence of detection in most cases. Factors such as the less favorable Strehl ratio in visible light and disk extinction at visible wavelengths can hinder their detection.

Surveys dedicated to looking for still accreting planets in the $H\alpha$ line have unfortunately been very challenging in the past (e.g., Cugno et al., 2019; Zurlo et al., 2020; Huéramo et al., 2022). The Strehl ratio is less favorable in visible light, and the disk extinction in the visible

can play a significant role. On the other hand, in the thermal infrared range, the contribution of circumplanetary material can enhance the signal at the planet’s location (see, e.g., Zhu et al., 2016). Furthermore, accreting protoplanets are expected to host circumplanetary disks (e.g., Aoyama et al., 2018). Therefore, younger planets have higher chances of detection at longer wavelengths due to the presence of circumplanetary disks and their high entropy during the first Myr of their formation. New instruments such as VLT/ERIS, JWST/NIRCAM, or, in the future, eELT/METIS will play a crucial role in detecting still-forming planets at longer wavelengths.

An alternative technique to look for protoplanets still embedded in their parent disk is the “disk kinematics” technique (Perez et al., 2015; Pérez et al., 2018), which allows to pinpoint the presence and locations of protoplanets via the footprint they stamp on the velocities of the gas in a disk. Recently we saw the first indirect detection using disk kinematics of a protoplanet (HD 163296 b; Pinte et al., 2018) and a protoplanet inside a gap (HD 97048 b; Pinte et al., 2019). This technique is now widely used in the international community and currently drives some of the most ambitious proposals for ALMA observations.

8 Brown dwarfs and exoplanets

Similar properties of the giant planets of the solar system are found in the so-called “substellar objects”: brown dwarfs (BDs) and planets. This class is composed of objects that are not massive enough to host nuclear fusion of hydrogen in the core. The upper limit of the mass for a substellar object is then $\sim 0.08 M_{\odot}$ ($84 M_{\text{Jup}}$). Objects in the mass range $11.0\text{--}16.3 M_{\text{Jup}}$ can fuse deuterium (Spiegel et al., 2011), and those above $\sim 65 M_{\text{Jup}}$ can fuse lithium (Lodders and Fegley, 2006). The boundary between a brown dwarf and a giant planet is still in debate. More studies will permit us to know whether the mechanisms of formation and/or the physics of the interior are different. Generally, the limit is imposed by the mass of the object for simplicity, but it should be given by the formation mechanism.

The class of substellar objects includes spectral types from late M to Y. The spectral types L and T were introduced by Kirkpatrick et al. (1999), for objects cooler than M-dwarfs. Then, Cushing et al. (2011) introduced the class of Y-type dwarfs, the coolest objects ever observed. The main features of substellar objects of the spectral sequence from M to T are shown in Fig. 18. The main properties of the spectral classes are:

- **M-dwarfs.** This spectral type is the link between stellar objects and BDs. The latest types of the M sequence include young objects which are considered BDs. The spectrum is characterized by the presence of TiO and VO. TiO bands increase in strength up to spectral type M6, and VO becomes strong in the latest types (Bailey, 2014). Broad absorptions due to H₂O are found around 1.4 and 1.9 μm , especially in later spectral types. Other molecules with strong absorption are FeH, CrH, and MgH.
- **L-dwarfs.** In this type of dwarfs, the TiO and the vanadium monoxide are increasingly disappearing. At their places, the bands of CrH, FeH, and alkaline metals appear in the optical. In the near-infrared, the bands of CO, CrH, and FeH are strong till the mid-L and then become weaker. The sequence of the L-dwarfs is redder than the others in the NIR mag/color diagram (see Fig. 19). This is due to the dusty clouds of species such as enstatite, forsterite, spinel, and solid iron which condense in the upper layers of the atmosphere (see, e.g., Allard et al., 2001).
- **T-dwarfs.** The T-dwarf class is characterized by the presence of methane (CH₄) absorption features in the near-IR region (1-2.5 μm) and water absorption bands. The methane absorptions at 1.6 and 2.2 μm (H and K bands) cause the blue shift of the sequence in the mag/color diagram (see Fig. 19). They have a closer resemblance to the solar system’s giant planets. Burgasser et al. (2002) estimate that, at birth, Jupiter had a T_{eff} near 600-1000 K and the appearance of a T-dwarf.
- **Y-dwarfs.** These objects lack water absorption bands because the H₂O condensates with temperatures around 500 K and it is not present in their clouds (Ackerman and Marley, 2001; Burrows et al., 2003).

Substellar objects are known to evolve with time more rapidly than low-mass stars. This is a fundamental property of these objects for the direct imaging technique, as in the first stages of their life they are much brighter and hotter, making their detection by HCI much easier. Since they do not have any significant internal source of energy, planets, and BDs cool down gradually with time. The evolution in time of the temperature for different masses is shown in Fig. 20. Brown dwarfs have an initial temperature of ~ 2500 K during the first 10 Myr, then they cool rapidly and the temperature can drop to 500 K after 10 Gyr. On the other hand, planets cool down since the beginning, reaching a final temperature of ~ 200 K after 1 Gyr. In the first stages, substellar objects are bright, large in radius, and usually fully adiabatic (as Jupiter).

The luminosity of substellar objects generally decreases with a power law (roughly $L \sim 1/t$). If we combine the information on the luminosity with the estimated age of the system, we can derive a mass for the companion. This value is only an estimated quantity from models if not coupled with dynamical information (from radial velocities, for example). Especially at young ages, models are not fully tested. Marley et al. (2007) proposed models where the initial conditions were not arbitrary but assumed by the core accretion scenario: the “cold-start” models. The two different formation scenarios seen in the previous Section 6, lead to different predictions on the luminosity of planets at the first stages. Planets formed by gravitational instability are expected to have large radii and high temperatures. The entropy of these objects is high. In the core accretion scenario, the birth of planets is more gentle, they have a low entropy, small radii and low

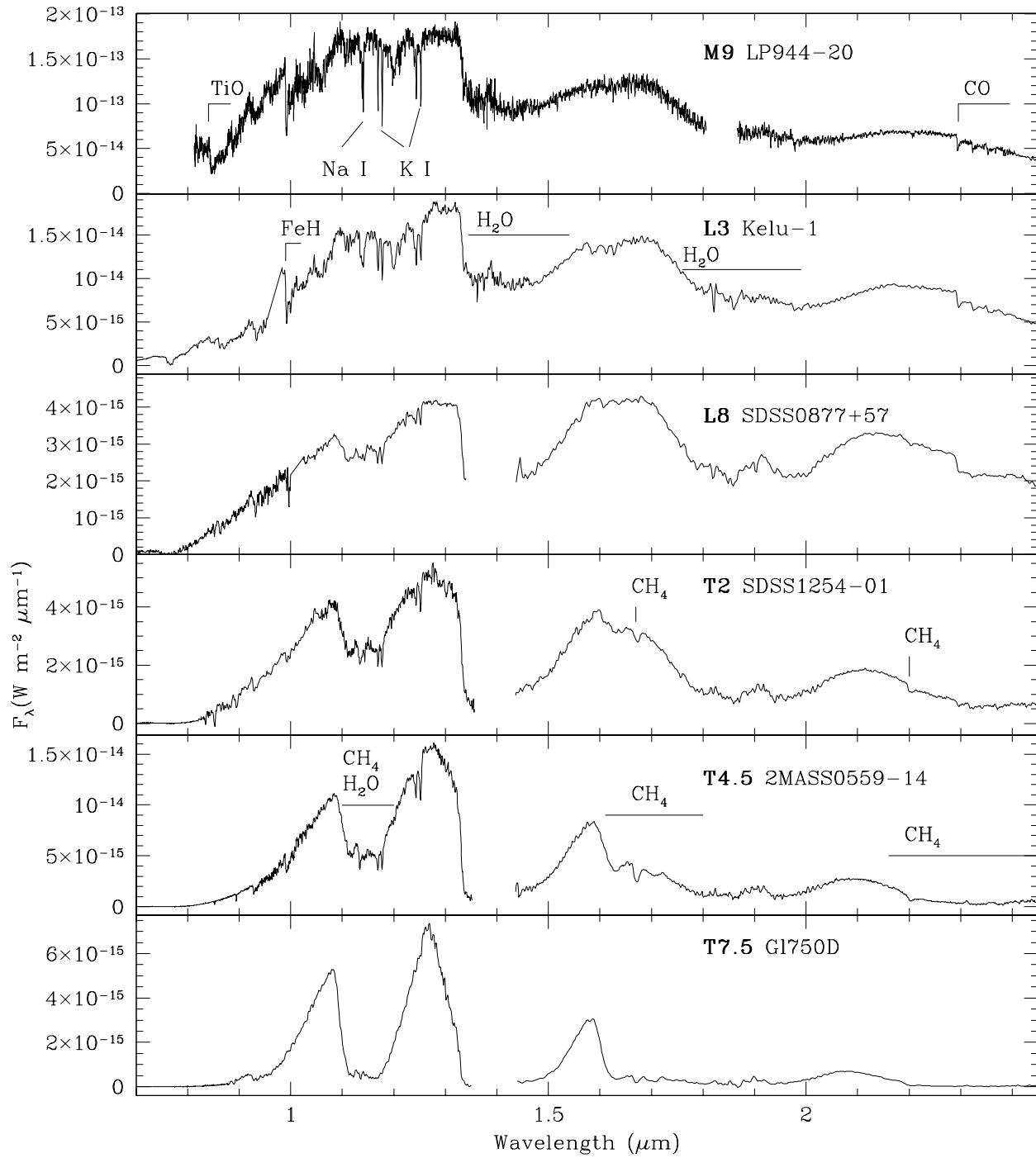


Fig. 18 Figure and caption taken from Bailey (2014), with references for the data therein. Spectra of ultracool dwarfs from M9 to T7.5. The species responsible for the main absorption features are indicated.

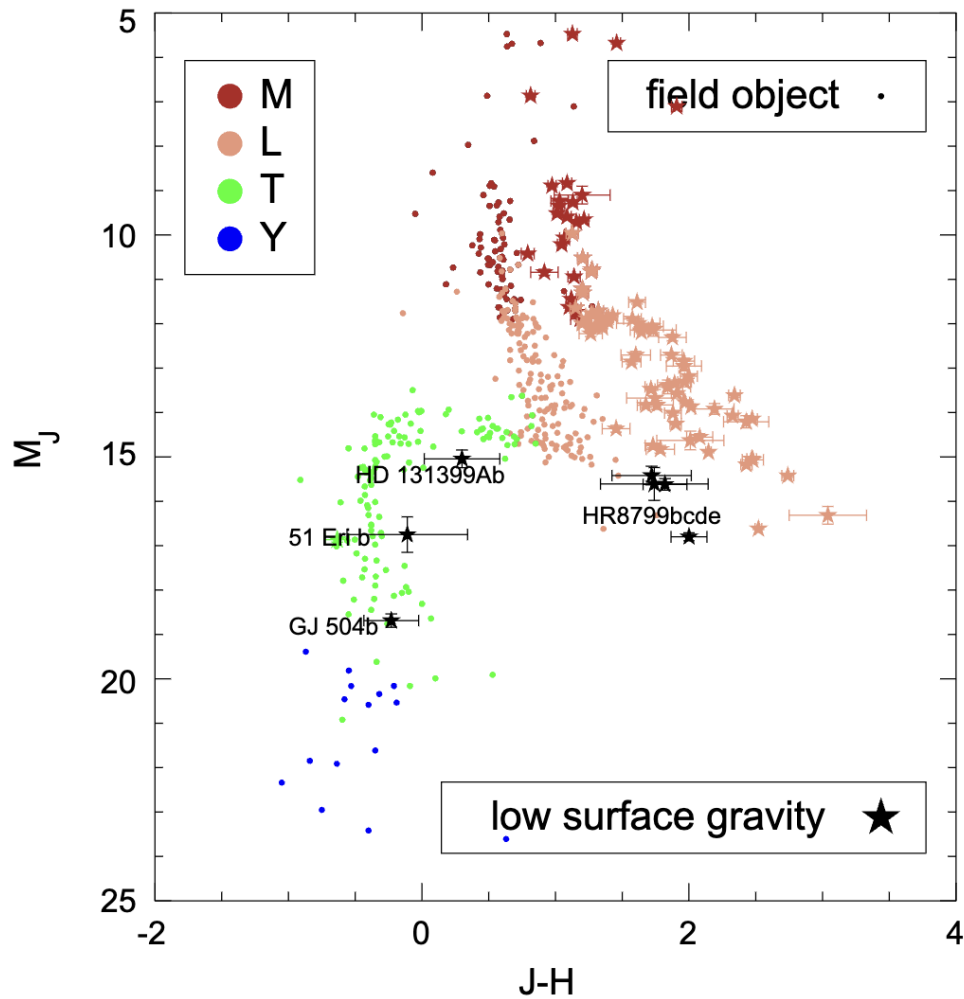


Fig. 19 Figure taken from Biller (2017), with references for the data therein. Color magnitude diagram ($J - H$ against absolute magnitude in J , M_J) for late-type dwarfs from spectral type M to Y. Some direct imaging companions are represented as black stars.

T_{eff} . The evolution of the three parameters is shown in Fig. 21 for both models. The plots show that planets keep the information of their formation just in the first Myr of their life, for old objects the two models are coincident. Spiegel and Burrows (2012) proposed a third scenario, called “warm-start”, which is in between the two former models. Direct imaging campaigns, possibly coupled to astrometric or RV information, are providing luminosities of newborn planets that will help to constrain and test these evolutionary tracks and better understand the mechanism of formation and evolution of substellar objects.

9 Conclusions and future perspectives

Direct imaging stands out as the exclusive technique capable of disentangling the light emitted by extrasolar planets from that of their parent stars. This method offers a unique opportunity to delve into the outer regions of planetary systems, for separations greater than 10 astronomical units from the host star—an exploration not feasible with indirect detection techniques. A key advantage of direct imaging lies in its ability to capture the spectra of these distant worlds, providing valuable insights into their composition and chemistry.

Moreover, direct imaging, when coupled with sufficient time coverage, facilitates the comprehensive determination of orbital parameters for the detected objects. This precision is particularly notable for close-in planets such as β Pic b. High-contrast imaging provides spectra from sub-stellar companions, a powerful instrument to investigate the properties of planetary atmospheres, cloud coverage, chemical abundances, etc.

The primary targets of high-contrast imaging are very young systems, as planets are self-luminous and bright during the first stages of their life. Direct imaging provides then a whole picture of a newly formed system, giving the opportunity to investigate which is the

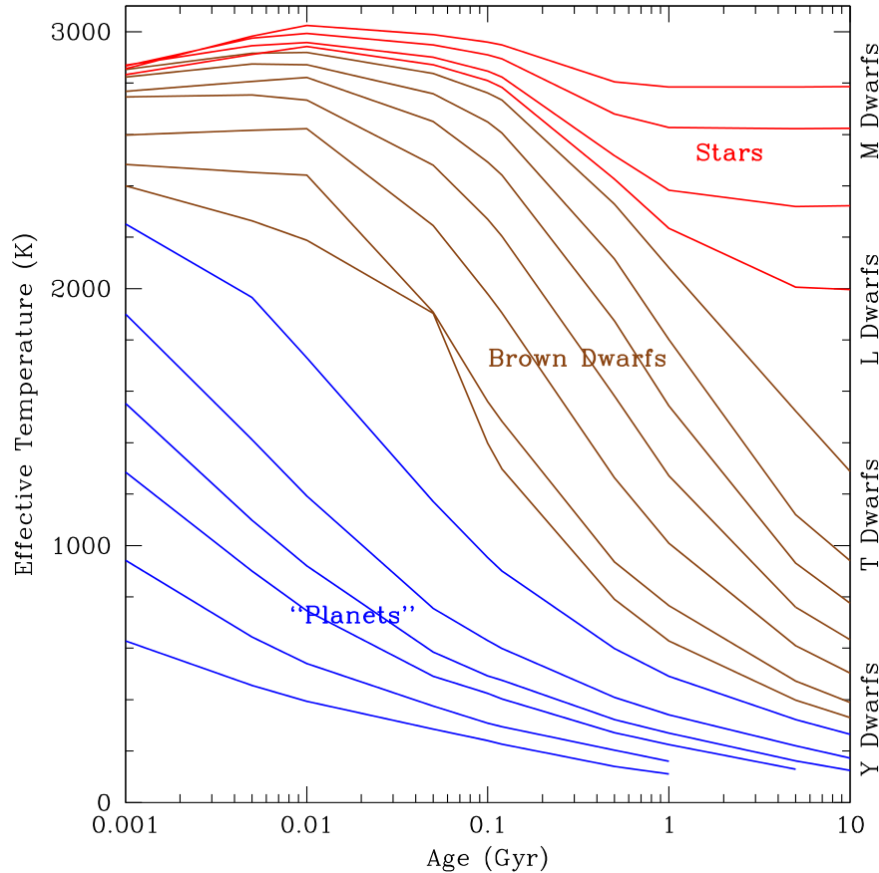


Fig. 20 Figure taken from Bailey (2014). Evolution of effective temperature for substellar objects. The range of mass represented goes from 0.0005 to 0.1 M_{\odot} based on the models of Baraffe et al. (2003). The red tracks are for stars with masses above the hydrogen-burning limit. The magenta tracks are for brown dwarfs and the blue tracks are for objects below the deuterium burning limit (planets or sub-brown dwarfs). The tracks plotted from top to bottom are masses of (Stars: 0.1, 0.09, 0.08, 0.075 M_{\odot}) (Brown Dwarfs: 0.07, 0.06, 0.05, 0.04, 0.03, 0.02, 0.015 M_{\odot}), (Planets: 0.01, 0.005, 0.003, 0.002, 0.001, 0.0005 M_{\odot}).

preferred mechanism of planet formation, a debate that still remains open.

In particular, the direct imaging captured photons of still-forming planets, or “protoplanets”, using mass accretion indicators as the $H\alpha$ line emission. Current detections are only a few due to the difficulty of disentangling the signal of a forming planet from a disk feature. The strongest detection to date is two accreting protoplanets around the young star PDS 70, which also hosts a gapped protoplanetary disk. Future detections will help us understand the mass formation rate of substellar companions and the location where planets form in a disk.

The future of direct imaging is promising. Instruments on board the James Webb Space Telescope are delivering their first spectacular results. JWST will permit thermal infrared (3–20 μm) observations of exoplanets, which are heavily affected by the thermal background for ground-based telescopes. From the ground, the instrument VLT/ERIS started its operations in 2022. ERIS includes a near-infrared camera that operates with the APP and vortex coronagraphs and is suitable for detecting exoplanets even around faint stars. The instrument can use a laser guide star to perform the observations.

The first light for the European Extremely Large Telescope (eELT) is foreseen for the year 2028. One of the first light instruments is METIS, a mid-infrared imager and spectrograph that will be equipped with coronagraphs to perform high-contrast imaging. After the first generation instruments, a dedicated planet finder, the planetary camera and spectrograph (PCS) instrument is foreseen to be installed in the eELT (Kasper et al., 2021). This instrument is specifically designed to image even Earth-size planets in the neighborhood of the Sun. Instruments from space and the ground will be able soon to directly detect planets with the mass of our Earth, with tremendous implications for the study of planetary systems, their formation, and evolution.

Acknowledgments

The author acknowledges support from ANID – Millennium Science Initiative Program – Center Code NCN2021_080.

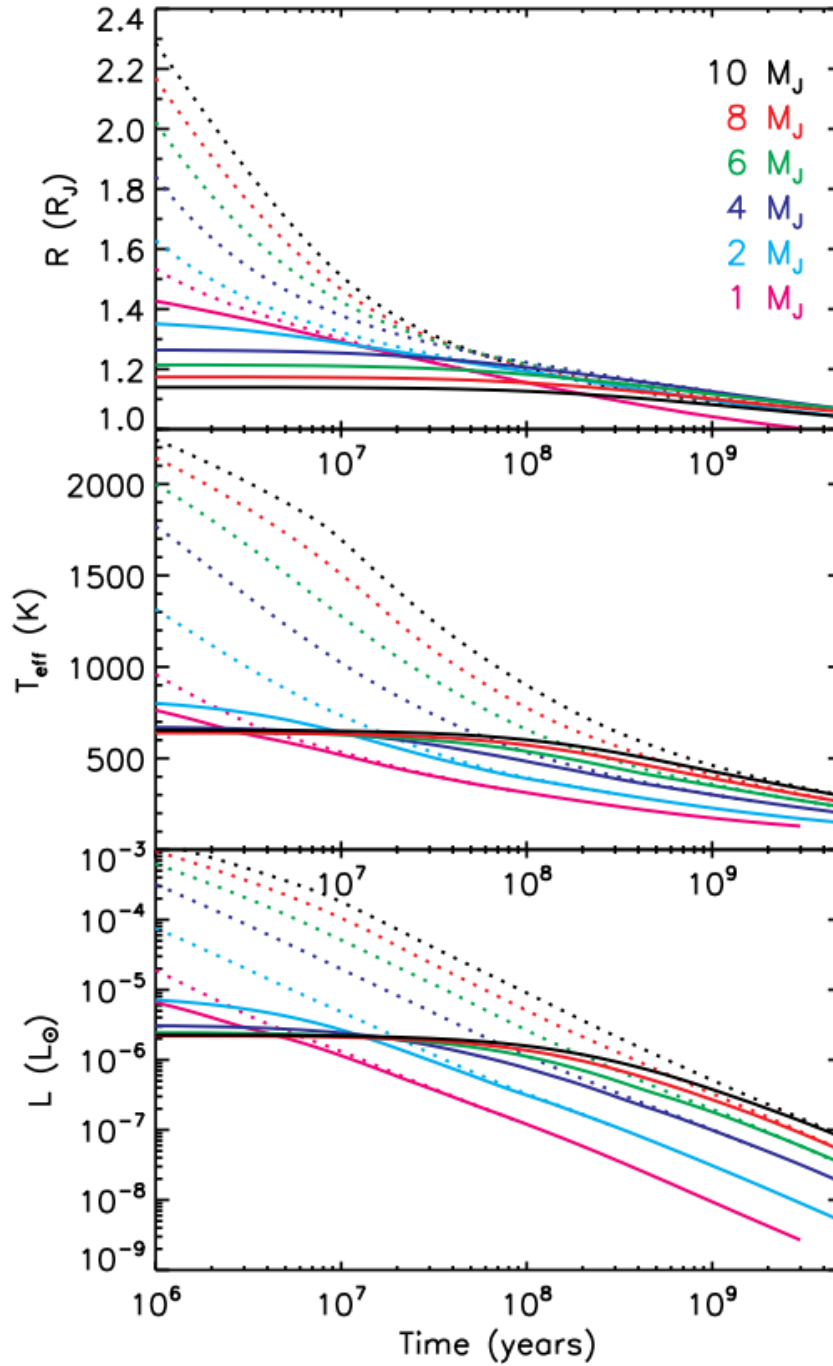


Fig. 21 Figure taken from Marley et al. (2007). Evolution of the parameters of radius, R , temperature, T_{eff} , and luminosity, L , for planets with different masses. “Hot-start” models are represented in dotted lines. The parameters for the two models converge for older ages. The moment when the planet loses the information on its birth depends on its mass.

See Also: The Protostars and Planet VII Chapter “Direct Imaging and Spectroscopy of Extrasolar Planets” by T. Currie et al. and “An Introduction to High Contrast Differential Imaging of Exoplanets and Disks” by K. Follette.

References

- Ackerman AS and Marley MS (2001), Aug. Precipitating Condensation Clouds in Substellar Atmospheres. *Astrophys. J.* 556: 872–884. doi:10.1086/321540. astro-ph/0103423.
- Alibert Y, Mordasini C and Benz W (2004), Apr. Migration and giant planet formation. *Astron. & Astrophys.* 417: L25–L28. doi:10.1051/0004-6361:20040053. astro-ph/0403574.
- Allard F, Hauschildt PH, Alexander DR, Tamanai A and Schweitzer A (2001), Jul. The Limiting Effects of Dust in Brown Dwarf Model Atmospheres. *Astrophys. J.* 556: 357–372. doi:10.1086/321547. astro-ph/0104256.
- Aoyama Y, Ikoma M and Tanigawa T (2018), Oct. Theoretical Model of Hydrogen Line Emission from Accreting Gas Giants. *Astrophys. J.* 866 (2), 84. doi:10.3847/1538-4357/aadc11. 1808.06776.
- Apai D, Kasper M, Skemer A, Hanson JR, Lagrange AM, Biller BA, Bonnefoy M, Buenzli E and Vigan A (2016), Mar. High-cadence, High-contrast Imaging for Exoplanet Mapping: Observations of the HR 8799 Planets with VLT/SPHERE Satellite-spot-corrected Relative Photometry. *Astrophys. J.* 820 (1), 40. doi:10.3847/0004-637X/820/1/40. 1602.02856.
- Armitage PJ (2007), Jan. Lecture notes on the formation and early evolution of planetary systems. *arXiv e-prints*, astro-ph/0701485doi:10.48550/arXiv.astro-ph/0701485. astro-ph/0701485.
- Bailey J (2014), Nov. The Dawes Review 3: The Atmospheres of Extrasolar Planets and Brown Dwarfs. *Publications of the Astronomical Society of Australia* 31, e043. doi:10.1017/pasa.2014.38. 1409.6821.
- Bailey V, Meshkat T, Reiter M, Morzinski K, Males J, Su KYL, Hinz PM, Kenworthy M, Stark D, Mamajek E, Briguglio R, Close LM, Follette KB, Puglisi A, Rodigas T, Weinberger AJ and Xompero M (2014), Jan. HD 106906 b: A Planetary-mass Companion Outside a Massive Debris Disk. *Astrophys. J. Lett.* 780, L4. doi:10.1088/2041-8205/780/1/L4. 1312.1265.
- Baraffe I, Chabrier G, Barman TS, Allard F and Hauschildt PH (2003), May. Evolutionary models for cool brown dwarfs and extrasolar giant planets. The case of HD 209458. *Astron. & Astrophys.* 402: 701–712. doi:10.1051/0004-6361:20030252. astro-ph/0302293.
- Baraffe I, Chabrier G and Barman T (2010), Jan. The physical properties of extra-solar planets. *Reports on Progress in Physics* 73 (1), 016901. doi:10.1088/0034-4885/73/1/016901. 1001.3577.
- Benisty M, Bae J, Facchini S, Keppler M, Teague R, Isella A, Kurtovic NT, Pérez LM, Sierra A, Andrews SM, Carpenter J, Czekala I, Dominik C, Henning T, Menard F, Pinilla P and Zurlo A (2021), Jul. A Circumplanetary Disk around PDS70c. *Astrophys. J. Lett.* 916 (1), L2. doi:10.3847/2041-8213/ac0f83. 2108.07123.
- Biller B (2017), Jan. The time domain for brown dwarfs and directly imaged giant exoplanets: the power of variability monitoring. *The Astronomical Review* 13 (1): 1–27. doi:10.1080/21672857.2017.1303105.
- Biller BA, Close LM, Masciadri E, Nielsen E, Lenzen R, Brandner W, McCarthy D, Hartung M, Kellner S, Mamajek E, Henning T, Miller D, Kenworthy M and Kulesa C (2007), Nov. An Imaging Survey for Extrasolar Planets around 45 Close, Young Stars with the Simultaneous Differential Imager at the Very Large Telescope and MMT. *Astrophys. J. Suppl.* 173: 143–165. doi:10.1086/519925.
- Biller BA, Apai D, Bonnefoy M, Desidera S, Gratton R, Kasper M, Kenworthy M, Lagrange AM, Lazzoni C, Mesa D, Vigan A, Wagner K, Vos JM and Zurlo A (2021), May. A high-contrast search for variability in HR 8799bc with VLT-SPHERE. *Mon. Not. Roy. Astron. Soc.* 503 (1): 743–767. doi:10.1093/mnras/stab202. 2101.08514.
- Bohn AJ, Ginski C, Kenworthy MA, Mamajek EE, Pecaut MJ, Mugrauer M, Vogt N, Adam C, Meshkat T, Reggiani M and Snik F (2021), Apr. Discovery of a directly imaged planet to the young solar analog YSES 2. *Astron. & Astrophys.* 648, A73. doi:10.1051/0004-6361/202140508. 2104.08285.
- Boley AC (2009), Apr. The Two Modes of Gas Giant Planet Formation. *Astrophys. J. Lett.* 695: L53–L57. doi:10.1088/0004-637X/695/1/L53. 0902.3999.
- Boss AP (1997). Giant planet formation by gravitational instability. *Science* 276: 1836–1839. doi:10.1126/science.276.5320.1836.
- Bowler BP, Liu MC, Mawet D, Ngo H, Malo L, Mace GN, McLane JN, Lu JR, Tristan II, Hinkley S, Hillenbrand LA, Shkolnik EL, Benneke B and Best WMJ (2017), Jan. Planets around Low-mass Stars (PALMS). VI. Discovery of a Remarkably Red Planetary-mass Companion to the AB Dor Moving Group Candidate 2MASS J22362452+4751425*. *Astron. J.* 153 (1), 18. doi:10.3847/1538-3881/153/1/18. 1611.00364.
- Burgasser AJ, Kirkpatrick JD, Brown ME, Reid IN, Burrows A, Liebert J, Matthews K, Gizis JE, Dahn CC, Monet DG, Cutri RM and Skrutskie MF (2002), Jan. The Spectra of T Dwarfs. I. Near-Infrared Data and Spectral Classification. *Astrophys. J.* 564 (1): 421–451. doi:10.1086/324033. astro-ph/0108452.
- Burgasser AJ, Simcoe RA, Bochanski JJ, Saumon D, Mamajek EE, Cushing MC, Marley MS, McMurtry C, Pipher JL and Forrest WJ (2010), Dec. Clouds in the Coldest Brown Dwarfs: Fire Spectroscopy of Ross 458C. *Astrophys. J.* 725: 1405–1420. doi:10.1088/0004-637X/725/2/1405. 1009.5722.
- Burrows A, Sudarsky D and Lunine JI (2003), Oct. Beyond the T Dwarfs: Theoretical Spectra, Colors, and Detectability of the Coolest Brown Dwarfs. *Astrophys. J.* 596: 587–596. doi:10.1086/377709. astro-ph/0304226.
- Cameron AGW (1978), Feb. Physics of the primitive solar accretion disk. *Moon and Planets* 18: 5–40. doi:10.1007/BF00896696.
- Carson J, Thalmann C, Janson M, Kozakis T, Bonnefoy M, Biller B, Schlieder J, Currie T, McElwain M, Goto M, Henning T, Brandner W, Feldt M, Kandori R, Kuzuhara M, Stevens L, Wong P, Gainey K, Fukagawa M, Kuwada Y, Brandt T, Kwon J, Abe L, Egner S, Grady C, Guyon O, Hashimoto J, Hayano Y, Hayashi M, Hayashi S, Hodapp K, Ishii M, Iye M, Knapp G, Kudo T, Kusakabe N, Matsuo T, Miyama S, Morino J, Moro-Martin A, Nishimura T, Pyo T, Serabyn E, Suto H, Suzuki R, Takami M, Takato N, Terada H, Tomono D, Turner E, Watanabe M, Wisniewski J, Yamada T, Takami H, Usuda T and Tamura M (2013), Feb. Direct Imaging Discovery of a “Super-Jupiter” around the Late B-type Star κ And. *Astrophys. J. Lett.* 763 (2), L32. doi:10.1088/2041-8205/763/2/L32. 1211.3744.
- Chauvin G, Lagrange AM, Dumas C, Zuckerman B, Mouillet D, Song I, Beuzit JL and Lowrance P (2004), Oct. A giant planet candidate near a young brown dwarf. Direct VLT/NACO observations using IR wavefront sensing. *Astron. & Astrophys.* 425: L29–L32. doi:10.1051/0004-6361:200400056. astro-ph/0409323.
- Chauvin G, Lagrange AM, Dumas C, Zuckerman B, Mouillet D, Song I, Beuzit JL and Lowrance P (2005a), Aug. Giant planet companion to 2MASSW J1207334-393254. *Astron. & Astrophys.* 438: L25–L28. doi:10.1051/0004-6361:200500116. astro-ph/0504659.
- Chauvin G, Lagrange AM, Zuckerman B, Dumas C, Mouillet D, Song I, Beuzit JL, Lowrance P and Bessell MS (2005b), Aug. A companion to AB Pic at the planet/brown dwarf boundary. *Astron. & Astrophys.* 438 (3): L29–L32. doi:10.1051/0004-6361:200500111. astro-ph/0504658.
- Chauvin G, Vigan A, Bonnefoy M, Desidera S, Bonavita M, Mesa D, Boccaletti A, Buenzli E, Carson J, Delorme P, Hagelberg J, Montagnier G,

- Mordasini C, Quanz SP, Segransan D, Thalmann C, Beuzit JL, Biller B, Covino E, Feldt M, Girard J, Gratton R, Henning T, Kasper M, Lagrange AM, Messina S, Meyer M, Mouillet D, Moutou C, Reggiani M, Schlieder JE and Zurlo A (2015), Jan. The VLT/NaCo large program to probe the occurrence of exoplanets and brown dwarfs at wide orbits. II. Survey description, results, and performances. *Astron. & Astrophys.* 573, A127. doi:10.1051/0004-6361/201423564. 1405.1560.
- Claudi R, Maire AL, Mesa D, Cheetham A, Fontanive C, Gratton R, Zurlo A, Avenhaus H, Bhowmik T, Biller B, Boccaletti A, Bonavita M, Bonnefoy M, Cascone E, Chauvin G, Delboulb e A, Desidera S, D'Orazi V, Feautrier P, Feldt M, Flammini Dotti F, Girard JH, Giro E, Janson M, Hagelberg J, Keppler M, Kopytova T, Lacour S, Lagrange AM, Langlois M, Lannier J, Le Coroller H, Menard F, Messina S, Meyer M, Millward M, Olofsson J, Pavlov A, Peretti S, Perrot C, Pinte C, Pragt J, Ramos J, Rochat S, Rodet L, Roelfsema R, Rouan D, Salter G, Schmidt T, Sissa E, Thebault P, Udry S and Vigan A (2019), Feb. SPHERE dynamical and spectroscopic characterization of HD 142527B. *Astron. & Astrophys.* 622, A96. doi:10.1051/0004-6361/201833990. 1812.07814.
- Close LM, Follette KB, Males JR, Puglisi A, Xompero M, Apai D, Najita J, Weinberger AJ, Morzinski K, Rodigas TJ, Hinz P, Bailey V and Brigguglio R (2014), Feb. Discovery of H α Emission from the Close Companion inside the Gap of Transitional Disk HD 142527. *Astrophys. J. Lett.* 781 (2), L30. doi:10.1088/2041-8205/781/2/L30. 1401.1273.
- Cugno G, Quanz SP, Hunziker S, Stolker T, Schmid HM, Avenhaus H, Baudoz P, Bohn AJ, Bonnefoy M, Buenzli E, Chauvin G, Cheetham A, Desidera S, Dominik C, Feautrier P, Feldt M, Ginski C, Girard JH, Gratton R, Hagelberg J, Hugot E, Janson M, Lagrange AM, Langlois M, Magnard Y, Maire AL, Menard F, Meyer M, Milli J, Mordasini C, Pinte C, Pragt J, Roelfsema R, Rigal F, Szul agyi J, van Boekel R, van der Plas G, Vigan A, Wahhaj Z and Zurlo A (2019), Feb. A search for accreting young companions embedded in circumstellar disks. High-contrast H α imaging with VLT/SPHERE. *Astron. & Astrophys.* 622, A156. doi:10.1051/0004-6361/201834170. 1812.06993.
- Currie T, Fukagawa M, Thalmann C, Matsumura S and Plavchan P (2012), Aug. Direct Detection and Orbital Analysis of the Exoplanets HR 8799 bcd from Archival 2005 Keck/NIRC2 Data. *Astrophys. J. Lett.* 755 (2), L34. doi:10.1088/2041-8205/755/2/L34. 1206.0483.
- Currie T, Daemgen S, Debes J, Lafreniere D, Itoh Y, Jayawardhana R, Ratzka T and Correia S (2014), Jan. Direct Imaging and Spectroscopy of a Candidate Companion Below/Near the Deuterium-burning Limit in the Young Binary Star System, ROXs 42B. *Astrophys. J. Lett.* 780, L30. doi:10.1088/2041-8205/780/2/L30. 1310.4825.
- Currie T, Cloutier R, Brittain S, Grady C, Burrows A, Muto T, Kenyon SJ and Kuchner MJ (2015), Dec. Resolving the HD 100546 Protoplanetary System with the Gemini Planet Imager: Evidence for Multiple Forming, Accreting Planets. *Astrophys. J. Lett.* 814 (2), L27. doi:10.1088/2041-8205/814/2/L27. 1511.02526.
- Currie T, Lawson K, Schneider G, Lyra W, Wisniewski J, Grady C, Guyon O, Tamura M, Kotani T, Kawahara H, Brandt T, Uyama T, Muto T, Dong R, Kudo T, Hashimoto J, Fukagawa M, Wagner K, Lozi J, Chilcote J, Tobin T, Groff T, Ward-Duong K, Januszewski W, Norris B, Tuthill P, van der Marel N, Sitko M, Deo V, Vievard S, Jovanovic N, Martinache F, Ratzka T and Skaf N (2022), Apr. Images of embedded Jovian planet formation at a wide separation around AB Aurigae. *Nature Astronomy* 6: 751–759. doi:10.1038/s41550-022-01634-x. 2204.00633.
- Currie T, Brandt GM, Brandt TD, Lacy B, Burrows A, Guyon O, Tamura M, Liu RY, Sagynbayeva S, Tobin T, Chilcote J, Groff T, Marois C, Thompson W, Murphy SJ, Kuzuhara M, Lawson K, Lozi J, Deo V, Vievard S, Skaf N, Uyama T, Jovanovic N, Martinache F, Kasdin NJ, Kudo T, McElwain M, Janson M, Wisniewski J, Hodapp K, Nishikawa J, Helminiak K, Kwon J and Hayashi M (2023), Apr. Direct imaging and astrometric detection of a gas giant planet orbiting an accelerating star. *Science* 380 (6641): 198–203. doi:10.1126/science.abo6192. 2212.00034.
- Cushing MC, Kirkpatrick JD, Gelino CR, Griffith RL, Skrutskie MF, Mainzer A, Marsh KA, Beichman CA, Burgasser AJ, Prato LA, Simcoe RA, Marley MS, Saumon D, Freedman RS, Eisenhardt PR and Wright EL (2011), Dec. The Discovery of Y Dwarfs using Data from the Wide-field Infrared Survey Explorer (WISE). *Astrophys. J.* 743, 50. doi:10.1088/0004-637X/743/1/50. 1108.4678.
- D'Angelo G, Durisen RH and Lissauer JJ (2011). Giant Planet Formation. 319–346.
- de Boer J, Langlois M, van Holstein RG, Girard JH, Mouillet D, Vigan A, Dohlen K, Snik F, Keller CU, Ginski C, Stam DM, Milli J, Wahhaj Z, Kasper M, Schmid HM, Rabou P, Gluck L, Hugot E, Perret D, Martinez P, Weber L, Saugage JF, Boccaletti A, Le Coroller H, Dominik C, Henning T, Lagadec E, M enard F, Turatto M, Udry S, Chauvin G, Feldt M and Beuzit JL (2020), Jan. Polarimetric imaging mode of VLT/SPHERE/IRDIS. I. Description, data reduction, and observing strategy. *Astron. & Astrophys.* 633, A63. doi:10.1051/0004-6361/201834989. 1909.13107.
- De Rosa RJ, Nielsen EL, Wahhaj Z, Ruffio JB, Kalas PG, Peck AE, Hirsch LA and Roberson W (2023), Apr. Direct imaging discovery of a super-Jovian around the young Sun-like star AF Leporis. *Astron. & Astrophys.* 672, A94. doi:10.1051/0004-6361/202345877. 2302.06332.
- Delorme P, Gagn e J, Girard JH, Lagrange AM, Chauvin G, Naud ME, Lafreniere D, Doyon R, Riedel A, Bonnefoy M and Malo L (2013), May. Direct-imaging discovery of a 12–14 Jupiter-mass object orbiting a young binary system of very low-mass stars. *Astron. & Astrophys.* 553, L5. doi:10.1051/0004-6361/201321169. 1303.4525.
- Dodson-Robinson SE and Salyk C (2011), Sep. Transitional Disks as Signposts of Young, Multiplanet Systems. *Astrophys. J.* 738 (2), 131. doi:10.1088/0004-637X/738/2/131. 1106.4824.
- Doelman DS, Snik F, Por EH, Bos SP, Otten GPPL, Kenworthy M, Haffert SY, Wilby M, Bohn AJ, Sutliff BJ, Miller K, Ouellet M, de Boer J, Keller CU, Escuti MJ, Shi S, Warriner NZ, Hornburg K, Birkby JL, Males J, Morzinski KM, Close LM, Codona J, Long J, Schatz L, Lumbres J, Rodack A, Van Gorkom K, Hedglen A, Guyon O, Lozi J, Groff T, Chilcote J, Jovanovic N, Thibault S, de Jonge C, Allain G, Vall ee C, Patel D, C ot e O, Marois C, Hinz P, Stone J, Skemer A, Briesemeister Z, Boehle A, Glauser AM, Taylor W, Baudoz P, Huby E, Absil O, Carlomagno B and Delacroix C (2021), Jul. Vector-apodizing phase plate coronagraph: design, current performance, and future development [Invited]. *AO* 60 (19): D52. doi:10.1364/AO.422155. 2104.11211.
- Dong R, Hall C, Rice K and Chiang E (2015), Oct. Spiral Arms in Gravitationally Unstable Protoplanetary Disks as Imaged in Scattered Light. *Astrophys. J. Lett.* 812 (2), L32. doi:10.1088/2041-8205/812/2/L32. 1510.00396.
- Esposito S, Mesa D, Skemer A, Arcidiacono C, Claudi RU, Desidera S, Gratton R, Mannucci F, Marzari F, Masciadri E, Close L, Hinz P, Kulesa C, McCarthy D, Males J, Agapito G, Argomedo J, Boutsia K, Brigguglio R, Brusa G, Busoni L, Cresci G, Fini L, Fontana A, Guerra JC, Hill JM, Miller D, Paris D, Pinna E, Puglisi A, Quiros-Pacheco F, Riccardi A, Stefanini P, Testa V, Xompero M and Woodward C (2013), Jan. LBT observations of the HR 8799 planetary system. First detection of HR 8799e in H band. *Astron. & Astrophys.* 549, A52. doi:10.1051/0004-6361/201219212. 1203.2735.
- Franson K, Bowler BP, Zhou Y, Pearce TD, Bardalez Gagliuffi DC, Biddle LI, Brandt TD, Crepp JR, Dupuy TJ, Faherty J, Jensen-Clem R, Morgan M, Sanghi A, Theissen CA, Tran QH and Wolf TN (2023), Jun. Astrometric Accelerations as Dynamical Beacons: A Giant Planet Imaged inside the Debris Disk of the Young Star AF Lep. *Astrophys. J. Lett.* 950 (2), L19. doi:10.3847/2041-8213/acad6f6. 2302.05420.
- Gaia Collaboration (2020), Nov. VizieR Online Data Catalog: Gaia EDR3 (Gaia Collaboration, 2020). *VizieR Online Data Catalog*, I/350doi:10.26093/cds/vizier.1350.
- Gaidos E, Hirano T, Kraus AL, Kuzuhara M, Zhang Z, Lee RA, Salama M, Berger TA, Grunblatt SK, Ansdell M, Liu MC, Harakawa H, Hodapp KW, Jacobson S, Konishi M, Kotani T, Kudo T, Kurokawa T, Nishikawa J, Omiya M, Serizawa T, Tamura M, Ueda A and Vievard S (2022), May. Zodi-
acal exoplanets in time (ZEIT) XII: a directly imaged planetary-mass companion to a young Taurus M dwarf star. *Mon. Not. Roy. Astron. Soc.* 512 (1): 583–601. doi:10.1093/mnras/stab3069. 2110.08655.

- Galicher R, Marois C, Zuckerman B and Macintosh B (2013), May. Fomalhaut b: Independent Analysis of the Hubble Space Telescope Public Archive Data. *Astrophys. J.* 769 (1), 42. doi:10.1088/0004-637X/769/1/42. 1210.6745.
- Goldreich P and Tremaine S (1980), Oct. Disk-satellite interactions. *Astrophys. J.* 241: 425–441. doi:10.1086/158356.
- Gratton R, Ligi R, Sissa E, Desidera S, Mesa D, Bonnefoy M, Chauvin G, Cheetham A, Feldt M, Lagrange AM, Langlois M, Meyer M, Vigan A, Boccaletti A, Janson M, Lazzoni C, Zurlo A, De Boer J, Henning T, D'Orazi V, Gluck L, Madec F, Jaquet M, Baudoz P, Fantinel D, Pavlov A and Wildi F (2019), Mar. Blobs, spiral arms, and a possible planet around HD 169142. *Astron. & Astrophys.* 623, A140. doi:10.1051/0004-6361/201834760. 1901.06555.
- GRAVITY Collaboration, Lacour S, Nowak M, Wang J, Pfuhl O, Eisenhauer F, Abuter R, Amorim A, Anugu N, Benisty M, Berger JP, Beust H, Blind N, Bonnefoy M, Bonnet H, Bourget P, Brandner W, Buron A, Collin C, Charnay B, Chapron F, Clénet Y, Coudé Du Foresto V, de Zeeuw PT, Deen C, Dembet R, Dexter J, Duvert G, Eckart A, Förster Schreiber NM, Fédou P, Garcia P, Garcia Lopez R, Gao F, Gendron E, Genzel R, Gillessen S, Gordo P, Greenbaum A, Habibi M, Haubois X, Haußmann F, Henning T, Hippler S, Horrobin M, Hubert Z, Jimenez Rosales A, Jocu L, Kendrick S, Kervella P, Kolb J, Lagrange AM, Lapeyrière V, Le Bouquin JB, Léna P, Lippa M, Lenzen R, Maire AL, Mollière P, Ott T, Paumard T, Perraut K, Perrin G, Pueyo L, Rabien S, Ramírez A, Rau C, Rodríguez-Coira G, Rousset G, Sanchez-Bermudez J, Scheithauer S, Schuhler N, Straub O, Straubmeier C, Sturm E, Tacconi LJ, Vincent F, van Dishoeck EF, von Fellenberg S, Wank I, Waisberg I, Widmann F, Wieprecht E, Wiest M, Wiezorrek E, Woillez J, Yazici S, Ziegler D and Zins G (2019), Mar. First direct detection of an exoplanet by optical interferometry. Astrometry and K-band spectroscopy of HR 8799 e. *Astron. & Astrophys.* 623, L11. doi:10.1051/0004-6361/201935253. 1903.11903.
- GRAVITY Collaboration, Nowak M, Lacour S, Mollière P, Wang J, Charnay B, van Dishoeck EF, Abuter R, Amorim A, Berger JP, Beust H, Bonnefoy M, Bonnet H, Brandner W, Buron A, Cantalloube F, Collin C, Chapron F, Clénet Y, Coudé Du Foresto V, de Zeeuw PT, Dembet R, Dexter J, Duvert G, Eckart A, Eisenhauer F, Förster Schreiber NM, Fédou P, Garcia Lopez R, Gao F, Gendron E, Genzel R, Gillessen S, Haußmann F, Henning T, Hippler S, Hubert Z, Jocu L, Kervella P, Lagrange AM, Lapeyrière V, Le Bouquin JB, Léna P, Maire AL, Ott T, Paumard T, Paladini C, Perraut K, Perrin G, Pueyo L, Pfuhl O, Rabien S, Rau C, Rodríguez-Coira G, Rousset G, Scheithauer S, Shangguan J, Straub O, Straubmeier C, Sturm E, Tacconi LJ, Vincent F, Widmann F, Wieprecht E, Wiezorrek E, Woillez J, Yazici S and Ziegler D (2020), Jan. Peering into the formation history of β Pictoris b with VLTI/GRAVITY long-baseline interferometry. *Astron. & Astrophys.* 633, A110. doi:10.1051/0004-6361/201936898. 1912.04651.
- Greenbaum AZ, Pueyo L, Ruffio JB, Wang JJ, De Rosa RJ, Aguilar J, Rameau J, Barman T, Marois C, Marley MS, Konopacky Q, Rajan A, Macintosh B, Ansdell M, Arriaga P, Bailey VP, Bulger J, Burrows AS, Chilcote J, Cotten T, Doyon R, Duchêne G, Fitzgerald MP, Follette KB, Gerard B, Goodsell SJ, Graham JR, Hiben P, Hung LW, Ingraham P, Kalas P, Larkin JE, Maire J, Marchis F, Metchev S, Millar-Blanchaer MA, Nielsen EL, Norton A, Oppenheimer R, Palmer D, Patience J, Perrin MD, Poyneer L, Rantakyö FT, Savransky D, Schneider AC, Sivaramakrishnan A, Song I, Soummer R, Thomas S, Wallace JK, Ward-Duong K, Wiktorowicz S and Wolff S (2018), Jun. GPI Spectra of HR 8799 c, d, and e from 1.5 to 2.4 μm with KLIP Forward Modeling. *Astron. J.* 155 (6), 226. doi:10.3847/1538-3881/aabcb8. 1804.07774.
- Guerri G, Robbe-Dubois S, Daban JB, Abe L, Douet R, Bendjoya P, Vakili F, Carbillat M, Beuzit JL, Puget P, Dohlen K and Mouillet D (2009), Jan. Apodized Lyot Coronagraph for VLT-SPHERE: Laboratory tests and performances of a first prototype in the visible. *ArXiv e-prints* 0901.2429.
- Guyon O, Pluzhnik EA, Kuchner MJ, Collins B and Ridgway ST (2006), Nov. Theoretical Limits on Extrasolar Terrestrial Planet Detection with Coronagraphs. *Astrophys. J. Suppl.* 167 (1): 81–99. doi:10.1086/507630. astro-ph/0608506.
- Haffert SY, Bohn AJ, de Boer J, Snellen IAG, Brinchmann J, Girard JH, Keller CU and Bacon R (2019), Jun. Two accreting protoplanets around the young star PDS 70. *Nature Astronomy* 3: 749–754. doi:10.1038/s41550-019-0780-5. 1906.01486.
- Hammond I, Christiaens V, Price DJ, Toci C, Pinte C, Juillard S and Garg H (2023), Jun. Confirmation and Keplerian motion of the gap-carving protoplanet HD 169142 b. *Mon. Not. Roy. Astron. Soc.* 522 (1): L51–L55. doi:10.1093/mnras/slad027. 2302.11302.
- Hourigan K and Ward WR (1984), Oct. Radial migration of preplanetary material - Implications for the accretion time scale problem. *Icarus* 60: 29–39. doi:10.1016/0019-1035(84)90136-2.
- Huélamo N, Chauvin G, Mendigutía I, Whelan E, Alcalá JM, Cugno G, Schmid HM, de Gregorio-Monsalvo I, Zurlo A, Barrado D, Benisty M, Quanz SP, Bouy H, Montesinos B, Beletsky Y and Szulagyi J (2022), Dec. Searching for H_{α} -emitting sources in the gaps of five transitional disks. SPHERE/ZIMPOL high-contrast imaging. *Astron. & Astrophys.* 668, A138. doi:10.1051/0004-6361/202243918. 2210.02212.
- Ingraham P, Marley MS, Saumon D, Marois C, Macintosh B, Barman T, Bauman B, Burrows A, Chilcote JK, De Rosa RJ, Dillon D, Doyon R, Dunn J, Erikson D, Fitzgerald MP, Gavel D, Goodsell SJ, Graham JR, Hartung M, Hiben P, Kalas PG, Konopacky Q, Larkin JA, Maire J, Marchis F, McBride J, Millar-Blanchaer M, Morzinski KM, Norton A, Oppenheimer R, Palmer DW, Patience J, Perrin MD, Poyneer LA, Pueyo L, Rantakyö F, Sadakuni N, Saddlemyer L, Savransky D, Soummer R, Sivaramakrishnan A, Song I, Thomas S, Wallace JK, Wiktorowicz SJ and Wolff SG (2014), Oct. Gemini Planet Imager Spectroscopy of the HR 8799 Planets c and d. *Astrophys. J. Lett.* 794 (1), L15. doi:10.1088/2041-8205/794/1/L15. 1409.5456.
- Isella A, Benisty M, Teague R, Bae J, Keppler M, Facchini S and Pérez L (2019), Jul. Detection of Continuum Submillimeter Emission Associated with Candidate Protoplanets. *Astrophys. J. Lett.* 879 (2), L25. doi:10.3847/2041-8213/ab2a12. 1906.06308.
- Itoh Y, Hayashi M, Tamura M, Tsuji T, Oasa Y, Fukagawa M, Hayashi SS, Naoi T, Ishii M, Mayama S, Morino Ji, Yamashita T, Pyo TS, Nishikawa T, Usuda T, Murakawa K, Suto H, Oya S, Takato N, Ando H, Miyama SM, Kobayashi N and Kaifu N (2005), Feb. A Young Brown Dwarf Companion to DH Tauri. *Astrophys. J.* 620 (2): 984–993. doi:10.1086/427086. astro-ph/0411177.
- Kalas P, Graham JR, Chiang E, Fitzgerald MP, Clampin M, Kite ES, Stapelfeldt K, Marois C and Krist J (2008), Nov. Optical Images of an Exosolar Planet 25 Light-Years from Earth. *Science* 322: 1345–. doi:10.1126/science.1166609. 0811.1994.
- Kalas P, Graham JR, Fitzgerald MP and Clampin M (2013), Sep. STIS Coronagraphic Imaging of Fomalhaut: Main Belt Structure and the Orbit of Fomalhaut b. *Astrophys. J.* 775, 56. doi:10.1088/0004-637X/775/1/56. 1305.2222.
- Kama M, Folsom CP and Pinilla P (2015), Oct. Fingerprints of giant planets in the photospheres of Herbig stars. *Astron. & Astrophys.* 582, L10. doi:10.1051/0004-6361/201527094. 1509.02741.
- Kasper M, Cerpa Urra N, Pathak P, Bonse M, Nousiainen J, Engler B, Heritier CT, Kammerer J, Leveratto S, Rajani C, Bristow P, Le Louarn M, Madec PY, Ströbele S, Verinaud C, Glauser A, Quanz SP, Helin T, Keller C, Snik F, Boccaletti A, Chauvin G, Mouillet D, Kulcsár C and Raynaud HF (2021), Mar. PCS — A Roadmap for Exoearth Imaging with the ELT. *The Messenger* 182: 38–43. doi:10.18727/0722-6691/5221. 2103.11196.
- Kennedy GM, Lovell JB, Kalas P and Fitzgerald MP (2023), Sep. ALMA and Keck analysis of Fomalhaut field sources: JWST's Great Dust Cloud is a background object. *Mon. Not. Roy. Astron. Soc.* 524 (2): 2698–2704. doi:10.1093/mnras/stad2058. 2305.10480.
- Kenworthy MA, Codona JL, Hinz PM, Angel JRP, Heinze A and Sivanandam S (2007), May. First On-Sky High-Contrast Imaging with an Apodizing Phase Plate. *Astrophys. J.* 660 (1): 762–769. doi:10.1086/513596. astro-ph/0702324.
- Keppler M, Benisty M, Müller A, Henning T, van Boekel R, Cantalloube F, Ginski C, van Holstein RG, Maire AL, Pohl A, Samland M, Avenhaus H, Baudino JL, Boccaletti A, de Boer J, Bonnefoy M, Chauvin G, Desidera S, Langlois M, Lazzoni C, Marleau GD, Mordasini C, Pawellek N, Stolker T, Vigan A, Zurlo A, Birnstiel T, Brandner W, Feldt M, Flock M, Girard J, Gratton R, Hagelberg J, Isella A, Janson M, Juhasz A, Kemmer J, Kral Q, Lagrange AM, Launhardt R, Matter A, Ménard F, Milli J, Mollière P, Olofsson J, Pérez L, Pinilla P, Pinte C, Quanz SP, Schmidt T, Udry

- S, Wahhaj Z, Williams JP, Buenzli E, Cudel M, Dominik C, Galicher R, Kasper M, Lannier J, Mesa D, Mouillet D, Peretti S, Perrot C, Salter G, Sissa E, Wildi F, Abe L, Antichi J, Augereau JC, Baruffolo A, Baudoz P, Bazzoni A, Beuzit JL, Blanchard P, Brems SS, Buey T, De Caprio V, Carillet M, Carle M, Cascone E, Cheetham A, Claudi R, Costille A, Delboulb e A, Dohlen K, Fantinel D, Feautrier P, Fusco T, Giro E, Gluck L, Gry C, Hubin N, Hugot E, Jaquet M, Le Mignant D, Llored M, Madec F, Magnard Y, Martinez P, Maurel D, Meyer M, M oller-Nilsson O, Moulin T, Mugnier L, Orign e A, Pavlov A, Perret D, Petit C, Pragt J, Puget P, Rabou P, Ramos J, Rigal F, Rochat S, Roelfsema R, Rousset G, Roux A, Salasnich B, Sauvage JF, Sevin A, Soenke C, Stadler E, Suarez M, Turatto M and Weber L (2018), Sep. Discovery of a planetary-mass companion within the gap of the transition disk around PDS 70. *Astron. & Astrophys.* 617, A44. doi:10.1051/0004-6361/201832957. 1806. 11568.
- Kirkpatrick JD, Reid IN, Liebert J, Cutri RM, Nelson B, Beichman CA, Dahn CC, Monet DG, Gizis JE and Skrutskie MF (1999), Jul. Dwarfs Cooler than "M": The Definition of Spectral Type "L" Using Discoveries from the 2 Micron All-Sky Survey (2MASS). *Astrophys. J.* 519 (2): 802–833. doi:10.1086/307414.
- Konopacky QM, Marois C, Macintosh BA, Galicher R, Barman TS, Metchev SA and Zuckerman B (2016), Aug. Astrometric Monitoring of the HR 8799 Planets: Orbit Constraints from Self-consistent Measurements. *Astron. J.* 152 (2), 28. doi:10.3847/0004-6256/152/2/28. 1604. 08157.
- Kratter KM, Matzner CD and Krumholz MR (2008), Jul. Global Models for the Evolution of Embedded, Accreting Protostellar Disks. *Astrophys. J.* 681: 375–390. doi:10.1086/587543. 0709. 4252.
- Kratter KM, Matzner CD, Krumholz MR and Klein RI (2010a), Jan. On the Role of Disks in the Formation of Stellar Systems: A Numerical Parameter Study of Rapid Accretion. *Astrophys. J.* 708: 1585–1597. doi:10.1088/0004-637X/708/2/1585. 0907. 3476.
- Kratter KM, Murray-Clay RA and Youdin AN (2010b), Feb. The Runts of the Litter: Why Planets Formed Through Gravitational Instability Can Only Be Failed Binary Stars. *Astrophys. J.* 710: 1375–1386. doi:10.1088/0004-637X/710/2/1375. 0909. 2644.
- Kuzuhara M, Tamura M, Kudo T, Janson M, Kandori R, Brandt TD, Thalmann C, Spiegel D, Biller B, Carson J, Hori Y, Suzuki R, Burrows A, Henning T, Turner EL, McElwain MW, Moro-Mart n A, Suenaga T, Takahashi YH, Kwon J, Lucas P, Abe L, Brandner W, Egner S, Feldt M, Fujiwara H, Goto M, Grady CA, Guyon O, Hashimoto J, Hayano Y, Hayashi M, Hayashi SS, Hodapp KW, Ishii M, Iyer M, Knapp GR, Matsuo T, Mayama S, Miyama S, Morino JI, Nishikawa J, Nishimura T, Kotani T, Kusakabe N, Pyo TS, Serabyn E, Suto H, Takami M, Takato N, Terada H, Tomono D, Watanabe M, Wisniewski JP, Yamada T, Takami H and Usuda T (2013), Sep. Direct Imaging of a Cold Jovian Exoplanet in Orbit around the Sun-like Star GJ 504. *Astrophys. J.* 774, 11. doi:10.1088/0004-637X/774/1/11. 1307. 2886.
- Lafreni re D, Doyon R, Marois C, Nadeau D, Oppenheimer BR, Roche PF, Rigaut F, Graham JR, Jayawardhana R, Johnstone D, Kalas PG, Macintosh B and Racine R (2007a), Dec. The Gemini Deep Planet Survey. *Astrophys. J.* 670 (2): 1367–1390. doi:10.1086/522826. 0705. 4290.
- Lafreni re D, Doyon R, Nadeau D, Artigau  , Marois C and Beaulieu M (2007b), Jun. Improving the Speckle Noise Attenuation of Simultaneous Spectral Differential Imaging with a Focal Plane Holographic Diffuser. *Astrophys. J.* 661 (2): 1208–1217. doi:10.1086/517604. astro-ph/0703093.
- Lafreni re D, Jayawardhana R and van Kerkwijk MH (2008), Dec. Direct Imaging and Spectroscopy of a Planetary-Mass Candidate Companion to a Young Solar Analog. *Astrophys. J. Lett.* 689: L153–L156. doi:10.1086/595870. 0809. 1424.
- Lagrange AM, Gratadour D, Chauvin G, Fusco T, Ehrenreich D, Mouillet D, Rousset G, Rouan D, Allard F, Gendron  , Charton J, Mugnier L, Rabou P, Montri J and Lacombe F (2009), Jan. A probable giant planet imaged in the β Pictoris disk. VLT/NaCo deep L-band imaging. *Astron. & Astrophys.* 493: L21–L25. doi:10.1051/0004-6361:200811325. 0811. 3583.
- Lagrange AM, Bonnefoy M, Chauvin G, Apai D, Ehrenreich D, Boccaletti A, Gratadour D, Rouan D, Mouillet D, Lacour S and Kasper M (2010), Jul. A Giant Planet Imaged in the Disk of the Young Star β Pictoris. *Science* 329: 57–. doi:10.1126/science.1187187. 1006. 3314.
- Lagrange AM, Meunier N, Rubini P, Keppler M, Galland F, Chapellier E, Michel E, Balona L, Beust H, Guillot T, Grandjean A, Borgniet S, M karnia D, Wilson PA, Kiefer F, Bonnefoy M, Lillo-Box J, Pantoja B, Jones M, Iglesias DP, Rodet L, Diaz M, Zapata A, Abe L and Schneider FX (2019), Aug. Evidence for an additional planet in the β Pictoris system. *Nature Astronomy* 3: 1135–1142. doi:10.1038/s41550-019-0857-1.
- Lagrange AM, Rubini P, Nowak M, Lacour S, Grandjean A, Boccaletti A, Langlois M, Delorme P, Gratton R, Wang J, Flasseur O, Galicher R, Kral Q, Meunier N, Beust H, Babusiaux C, Le Coroller H, Thebaud F, Kervella P, Zurlo A, Maire AL, Wahhaj Z, Amorin A, Asensio-Torres R, Benisty M, Berger JP, Bonnefoy M, Brandner W, Cantalloube F, Charnay B, Chauvin G, Choquet E, Cl eney Y, Christiaens V, Coud  Du Foresto V, de Zeeuw PT, Desidera S, Duvert G, Eckart A, Eisenhauer F, Galland F, Gao F, Garcia P, Garcia Lopez R, Gendron E, Genzel R, Gillissen S, Girard J, Hagelberg J, Haubois X, Henning T, Heissel G, Hippler S, Horrobin M, Janson M, Kammerer J, Kenworthy M, Keppler M, Kreidberg L, Lapeyre V, Le Bouquin JB, L na P, M rand A, Messina S, Molli re S, Molli re JD, Ott T, Otten G, Paumard T, Paladini C, Perraut K, Perrin G, Pueyo L, Pfuhl O, Rodet L, Rodr guez-Coira G, Rousset G, Samland M, Shangguan J, Schmidt T, Straub O, Straubmeier C, Stolker T, Vigan A, Vincent F, Widmann F, Woillez J and GRAVITY Collaboration (2020), Oct. Unveiling the β Pictoris system, coupling high contrast imaging, interferometric, and radial velocity data. *Astron. & Astrophys.* 642, A18. doi:10.1051/0004-6361/202038823.
- Lin DNC and Papaloizou J (1986), Oct. On the Tidal Interaction between Protoplanets and the Protoplanetary Disk. III. Orbital Migration of Protoplanets. *Astrophys. J.* 309: 846. doi:10.1086/164653.
- Lodders K and Fegley Jr. B (2006). Chemistry of Low Mass Substellar Objects. pp. 1. doi:10.1007/3-540-30313-8-1.
- Luhman KL, Burgasser AJ and Bochanski JJ (2011), Mar. Discovery of a Candidate for the Coolest Known Brown Dwarf. *Astrophys. J. Lett.* 730, L9. doi:10.1088/2041-8205/730/1/L9. 1102. 5411.
- Macintosh B, Graham JR, Barman T, De Rosa RJ, Konopacky Q, Marley MS, Marois C, Nielsen EL, Pueyo L, Rajan A, Rameau J, Saumon D, Wang JJ, Patience J, Ammons M, Arriaga P, Artigau E, Beckwith S, Brewster J, Bruzzone S, Bulger J, Burningham B, Burrows AS, Chen C, Chiang E, Chilcote JK, Dawson RI, Dong R, Doyon R, Draper ZH, Duch ne G, Esposito TM, Fabrycky D, Fitzgerald MP, Follette KB, Fortney JJ, Gerard B, Goodsell S, Greenbaum AZ, Hibon P, Hinkley S, Cotten TH, Hung LW, Ingraham P, Johnson-Groh M, Kalas P, Lafreniere D, Larkin JE, Lee J, Line M, Long D, Maire J, Marchis F, Matthews BC, Max CE, Metchev S, Millar-Blanchaer MA, Mittal T, Morley CV, Morzinski KM, Murray-Clay R, Oppenheimer R, Palmer DW, Patel R, Perrin MD, Poyneer LA, Rafikov RR, Rantakyr  FT, Rice EL, Rojo P, Rudy AR, Ruffio JB, Ruiz MT, Sadakuni N, Saddlemyer L, Salama M, Savransky D, Schneider AC, Sivaramakrishnan A, Song I, Soummer R, Thomas S, Vasisth G, Wallace JK, Ward-Duong K, Wiktorowicz SJ, Wolff SG and Zuckerman B (2015), Oct. Discovery and spectroscopy of the young jovian planet 51 Eri b with the Gemini Planet Imager. *Science* 350 (6256): 64–67. doi:10.1126/science.aac5891. 1508. 03084.
- Maire AL, Skemer AJ, Hinz PM, Desidera S, Esposito S, Gratton R, Marzari F, Skrutskie MF, Biller BA, Defr re D, Bailey VP, Leisenring JM, Apai D, Bonnefoy M, Brandner W, Buenzli E, Claudi RU, Close LM, Crepp JR, De Rosa RJ, Eisner JA, Fortney JJ, Henning T, Hofmann KH, Kopytova TG, Males RJ, Mesa D, Morzinski KM, Oza A, Patience J, Pinna E, Rajan A, Schertl D, Schlieder JE, Su KYL, Vaz A, Ward-Duong K, Weigelt G and Woodward CE (2015), Apr. The LEECH Exoplanet Imaging Survey. Further constraints on the planet architecture of the HR 8799 system. *Astron. & Astrophys.* 576, A133. doi:10.1051/0004-6361/201425185. 1412. 6989.
- Marley MS, Fortney JJ, Hubickyj O, Bodenheimer P and Lissauer JJ (2007), Jan. On the Luminosity of Young Jupiters. *Astrophys. J.* 655 (1): 541–549. doi:10.1086/509759. astro-ph/0609739.
- Marley MS, Saumon D, Cushing M, Ackerman AS, Fortney JJ and Freedman R (2012), Aug. Masses, Radii, and Cloud Properties of the HR 8799 Planets. *Astrophys. J.* 754 (2), 135. doi:10.1088/0004-637X/754/2/135. 1205. 6488.
- Marois C, Doyon R, Racine R and Nadeau D (2000), Jan. Efficient Speckle Noise Attenuation in Faint Companion Imaging. *Pub. Astron. Soc. Pacific* 112: 91–96. doi:10.1086/316492.

- Marois C, Lafrenière D, Doyon R, Macintosh B and Nadeau D (2006), Apr. Angular Differential Imaging: A Powerful High-Contrast Imaging Technique. *Astrophys. J.* 641: 556–564. doi:10.1086/500401. astro-ph/0512335.
- Marois C, Macintosh B, Barman T, Zuckerman B, Song I, Patience J, Lafrenière D and Doyon R (2008), Nov. Direct Imaging of Multiple Planets Orbiting the Star HR 8799. *Science* 322: 1348–. doi:10.1126/science.1166585. 0811.2606.
- Marois C, Zuckerman B, Konopacky QM, Macintosh B and Barman T (2010), Dec. Images of a fourth planet orbiting HR 8799. *Nature* 468: 1080–1083. doi:10.1038/nature09684. 1011.4918.
- Mawet D, Serabyn E, Liewer K, Hanot C, McEldowney S, Shemo D and O'Brien N (2009), Feb. Optical Vectorial Vortex Coronagraphs using Liquid Crystal Polymers: theory, manufacturing and laboratory demonstration. *Optics Express* 17: 1902–1918. doi:10.1364/OE.17.001902. 0912.0311.
- McLean IS, (Ed.) (1997). Electronic imaging in astronomy. Detectors and instrumentation.
- Mesa D, Gratton R, Kervella P, Bonavita M, Desidera S, D'Orazi V, Marino S, Zurlo A and Rigliaco E (2023), Apr. AF Lep b: The lowest-mass planet detected by coupling astrometric and direct imaging data. *Astron. & Astrophys.* 672, A93. doi:10.1051/0004-6361/202345865. 2302.06213.
- Miret-Roig N, Galli PAB, Brandner W, Bouy H, Barrado D, Olivares J, Antoja T, Romero-Gómez M, Figueras F and Lillo-Box J (2020), Oct. Dynamical traceback age of the β Pictoris moving group. *Astron. & Astrophys.* 642, A179. doi:10.1051/0004-6361/202038765. 2007.10997.
- Mizuno H (1980), Aug. Formation of the Giant Planets. *Progress of Theoretical Physics* 64: 544–557. doi:10.1143/PTP.64.544.
- Mohanty S, Jayawardhana R, Huélamo N and Mamajek E (2007), Mar. The Planetary Mass Companion 2MASS 1207-3932B: Temperature, Mass, and Evidence for an Edge-on Disk. *Astrophys. J.* 657 (2): 1064–1091. doi:10.1086/510877. astro-ph/0610550.
- Montesinos M, Cuadra J, Perez S, Baruteau C and Casassus S (2015), Jun. Protoplanetary Disks Including Radiative Feedback from Accreting Planets. *Astrophys. J.* 806 (2), 253. doi:10.1088/0004-637X/806/2/253. 1505.03392.
- Mordasini C (2013), Oct. Luminosity of young Jupiters revisited. Massive cores make hot planets. *Astron. & Astrophys.* 558, A113. doi:10.1051/0004-6361/201321617. 1306.5746.
- Mordasini C, Alibert Y, Benz W and Naef D (2008), Giant Planet Formation by Core Accretion, Fischer D, Rasio FA, Thorsett SE and Wolszczan A, (Eds.), *Extreme Solar Systems*, Astronomical Society of the Pacific Conference Series, 398, pp. 235, 0710.5667.
- Müller A, Keppler M, Henning T, Samland M, Chauvin G, Beust H, Maire AL, Molaverdikhani K, van Boekel R, Benisty M, Boccaletti A, Bonnefoy M, Cantalloube F, Charnay B, Baudino JL, Gennaro M, Long ZC, Cheetham A, Desidera S, Feldt M, Fusco T, Girard J, Gratton R, Hagelberg J, Janson M, Lagrange AM, Langlois M, Lazzoni C, Ligi R, Ménard F, Mesa D, Meyer M, Mollière P, Mordasini C, Moulin T, Pavlov A, Pawellek N, Quanz SP, Ramos J, Rouan D, Sissa E, Stadler E, Vigan A, Wahhaj Z, Weber L and Zurlo A (2018), Sep. Orbital and atmospheric characterization of the planet within the gap of the PDS 70 transition disk. *Astron. & Astrophys.* 617, L2. doi:10.1051/0004-6361/201833584. 1806.11567.
- Naud ME, Artigau É, Malo L, Albert L, Doyon R, Lafrenière D, Gagné J, Saumon D, Morley CV, Allard F, Homeier D, Beichman CA, Gelino CR and Boucher A (2014), May. Discovery of a Wide Planetary-mass Companion to the Young M3 Star GU Psc. *Astrophys. J.* 787, 5. doi:10.1088/0004-637X/787/1/5. 1405.2932.
- Neuhäuser R, Hohle MM, Ginski C, Schmidt JG, Hambaryan VV and Schmidt TOB (2015), Mar. The companion candidate near Fomalhaut - a background neutron star? *Mon. Not. Roy. Astron. Soc.* 448 (1): 376–389. doi:10.1093/mnras/stu2751. 1501.07083.
- Nielsen EL, Close LM, Biller BA, Masciadri E and Lenzen R (2008), Feb. Constraints on Extrasolar Planet Populations from VLT NACO/SDI and MMT SDI and Direct Adaptive Optics Imaging Surveys: Giant Planets are Rare at Large Separations. *Astrophys. J.* 674: 466–481. doi:10.1086/524344. 0706.4331.
- Nielsen EL, De Rosa RJ, Macintosh B, Wang JJ, Ruffio JB, Chiang E, Marley MS, Saumon D, Savransky D, Ammons SM, Bailey VP, Barman T, Blain C, Bulger J, Burrows A, Chilcote J, Cotten T, Czekala I, Doyon R, Duchêne G, Esposito TM, Fabrycky D, Fitzgerald MP, Follette KB, Fortney JJ, Gerard BL, Goodsell SJ, Graham JR, Greenbaum AZ, Hibon P, Hinkley S, Hirsch LA, Hom J, Hung LW, Dawson RI, Ingraham P, Kalas P, Konopacky Q, Larkin JE, Lee EJ, Lin JW, Maire J, Marchis F, Marois C, Metchev S, Millar-Blanchaer MA, Morzinski KM, Oppenheimer R, Palmer D, Patience J, Perrin M, Poyneer L, Pueyo L, Rafikov RR, Rajan A, Rameau J, Rantakyö FT, Ren B, Schneider AC, Sivaramakrishnan A, Song I, Soummer R, Tallis M, Thomas S, Ward-Duong K and Wolff S (2019), Jul. The Gemini Planet Imager Exoplanet Survey: Giant Planet and Brown Dwarf Demographics from 10 to 100 au. *Astron. J.* 158 (1), 13. doi:10.3847/1538-3881/ab16e9. 1904.05358.
- Nowak M, Lacour S, Lagrange AM, Rubini P, Wang J, Stolker T, Abuter R, Amorim A, Asensio-Torres R, Bauböck M, Benisty M, Berger JP, Beust H, Blunt S, Boccaletti A, Bonnefoy M, Bonnet H, Brandner W, Cantalloube F, Charnay B, Choquet E, Christiaens V, Clénet Y, Coudé Du Foresto V, Cridland A, de Zeeuw PT, Dembet R, Dexter J, Drescher A, Duvert G, Eckart A, Eisenhauer F, Gao F, Garcia P, Garcia Lopez R, Gardner T, Gendron E, Genzel R, Gillessen S, Girard J, Grandjean A, Haubois X, Heißel G, Henning T, Hinkley S, Hippler S, Horrobin M, Houllé M, Hubert Z, Jiménez-Rosales A, Jocou L, Kammerer J, Kervella P, Keppler M, Kreidberg L, Kulikauskas M, Lapeyrière V, Le Bouquin JM, Léna P, Mérand A, Maire AL, Mollière P, Monnier JD, Mouillet D, Müller A, Nasedkin E, Ott T, Otten G, Paumard T, Paladini C, Perraut K, Perrin G, Pueyo L, Pfuhl O, Rameau J, Rodet L, Rodríguez-Coira G, Rousset G, Scheithauer S, Shangguan J, Stadler J, Straub O, Straubmeier C, Sturm E, Tacconi LJ, van Dishoeck EF, Vigan A, Vincent F, von Fellenberg SD, Ward-Duong K, Widmann F, Wieprecht E, Wierzorrek E, Woillez J and GRAVITY Collaboration (2020), Oct. Direct confirmation of the radial-velocity planet β Pictoris c. *Astron. & Astrophys.* 642, L2. doi:10.1051/0004-6361/202039039. 2010.04442.
- Oppenheimer BR and Hinkley S (2009), Sep. High-Contrast Observations in Optical and Infrared Astronomy. *Ann. Rev. Astron. Astrophys.* 47: 253–289. doi:10.1146/annurev-astro-082708-101717. 0903.4466.
- Oppenheimer BR, Baranec C, Beichman C, Brenner D, Burruss R, Cady E, Crepp JR, Dekany R, Fergus R, Hale D, Hillenbrand L, Hinkley S, Hogg DW, King D, Ligon ER, Lockhart T, Nilsson R, Parry IR, Pueyo L, Rice E, Roberts JE, Roberts Jr. LC, Shao M, Sivaramakrishnan A, Soummer R, Truong T, Vasisht G, Veicht A, Vescelus F, Wallace JK, Zhai C and Zimmerman N (2013), May. Reconnaissance of the HR 8799 Exosolar System. I. Near-infrared Spectroscopy. *Astrophys. J.* 768, 24. doi:10.1088/0004-637X/768/1/24. 1303.2627.
- Pecaut MJ and Mamajek EE (2016), Sep. The star formation history and accretion-disc fraction among the Scorpius-Centaurus OB association. *Mon. Not. Roy. Astron. Soc.* 461 (1): 794–815. doi:10.1093/mnras/stw1300. 1605.08789.
- Perez S, Dunhill A, Casassus S, Roman P, Szulágyi J, Flores C, Marino S and Montesinos M (2015), Sep. Planet Formation Signposts: Observability of Circumplanetary Disks via Gas Kinematics. *Astrophys. J. Lett.* 811 (1), L5. doi:10.1088/2041-8205/811/1/L5. 1505.06808.
- Pérez S, Casassus S and Benítez-Llambay P (2018), Oct. Observability of planet-disc interactions in CO kinematics. *Mon. Not. Roy. Astron. Soc.* 480 (1): L12–L17. doi:10.1093/mnras/sly109. 1806.05125.
- Perryman M (2014), Jan. The Exoplanet Handbook.
- Petit dit de la Roche DJM, van den Ancker ME, Kissler-Patig M, Ivanov VD and Fedele D (2020), Jan. New constraints on the HR 8799 planetary system from mid-infrared direct imaging. *Mon. Not. Roy. Astron. Soc.* 491 (2): 1795–1799. doi:10.1093/mnras/stz3117. 1911.04814.
- Pinte C, Price DJ, Ménard F, Duchêne G, Dent WRF, Hill T, de Gregorio-Monsalvo I, Hales A and Mentiplay D (2018), Jun. Kinematic Evidence for an Embedded Protoplanet in a Circumstellar Disk. *Astrophys. J. Lett.* 860 (1), L13. doi:10.3847/2041-8213/aac6dc. 1805.10293.
- Pinte C, van der Plas G, Ménard F, Price DJ, Christiaens V, Hill T, Mentiplay D, Ginski C, Choquet E, Boehler Y, Duchêne G, Perez S and

- Casassus S (2019), Aug. Kinematic detection of a planet carving a gap in a protoplanetary disk. *Nature Astronomy* 3: 1109–1114. doi:10.1038/s41550-019-0852-6. 1907.02538.
- Pollack JB, Hubickyj O, Bodenheimer P, Lissauer JJ, Podolak M and Greenzweig Y (1996), Nov. Formation of the Giant Planets by Concurrent Accretion of Solids and Gas. *Icarus* 124: 62–85. doi:10.1006/icar.1996.0190.
- Pueyo L, Soummer R, Hoffmann J, Oppenheimer R, Graham JR, Zimmerman N, Zhai C, Wallace JK, Vescelus F, Veicht A, Vasisht G, Truong T, Sivaramakrishnan A, Shao M, Roberts L. C. J, Roberts JE, Rice E, Parry IR, Nilsson R, Lockhart T, Ligon ER, King D, Hinkley S, Hillenbrand L, Hale D, Dekany R, Crepp JR, Cady E, Burruss R, Brenner D, Beichman C and Baranec C (2015), Apr. Reconnaissance of the HR 8799 Exosolar System. II. Astrometry and Orbital Motion. *Astrophys. J.* 803 (1), 31. doi:10.1088/0004-637X/803/1/31. 1409.6388.
- Quanz SP, Amara A, Meyer MR, Kenworthy MA, Kasper M and Girard JH (2013), Mar. A Young Protoplanet Candidate Embedded in the Circumstellar Disk of HD 100546. *Astrophys. J. Lett.* 766, L1. doi:10.1088/2041-8205/766/1/L1. 1302.7122.
- Racine R, Walker GAH, Nadeau D, Doyon R and Marois C (1999), May. Speckle Noise and the Detection of Faint Companions. *Pub. Astron. Soc. Pacific* 111: 587–594. doi:10.1086/316367.
- Rameau J, Chauvin G, Lagrange AM, Boccaletti A, Quanz SP, Bonnefoy M, Girard JH, Delorme P, Desidera S, Klahr H, Mordasini C, Dumas C and Bonavita M (2013), Aug. Discovery of a Probable 4-5 Jupiter-mass Exoplanet to HD 95086 by Direct Imaging. *Astrophys. J. Lett.* 772 (2), L15. doi:10.1088/2041-8205/772/2/L15. 1305.7428.
- Rameau J, Follette KB, Pueyo L, Marois C, Macintosh B, Millar-Blanchaer M, Wang JJ, Vega D, Doyon R, Lafrenière D, Nielsen EL, Bailey V, Chilcote JK, Close LM, Esposito TM, Males JR, Metchev S, Morzinski KM, Ruffio JB, Wolff SG, Ammons SM, Barman TS, Bulger J, Cotten T, De Rosa RJ, Duchene G, Fitzgerald MP, Goodsell S, Graham JR, Greenbaum AZ, Higon P, Hung LW, Ingraham P, Kalas P, Konopacky Q, Larkin JE, Maire J, Marchis F, Oppenheimer R, Palmer D, Patience J, Perrin MD, Poyneer L, Rajan A, Rantakyro FT, Marley MS, Savransky D, Schneider AC, Sivaramakrishnan A, Song I, Soummer R, Thomas S, Wallace JK, Ward-Duong K and Wiktorowicz S (2017), Jun. An Optical/Near-infrared Investigation of HD 100546 b with the Gemini Planet Imager and MagAO. *Astron. J.* 153 (6), 244. doi:10.3847/1538-3881/aa6cae. 1704.06317.
- Rigliaco E, Natta A, Testi L, Randich S, Alcalà JM, Covino E and Stelzer B (2012), Dec. X-shooter spectroscopy of young stellar objects. I. Mass accretion rates of low-mass T Tauri stars in σ Orionis. *Astron. & Astrophys.* 548, A56. doi:10.1051/0004-6361/201219832. 1209.5799.
- Rouan D, Riaud P, Boccaletti A, Clénet Y and Labeyrie A (2000), Nov. The Four-Quadrant Phase-Mask Coronagraph. I. Principle. *Pub. Astron. Soc. Pacific* 112: 1479–1486. doi:10.1086/317707.
- Ruffio JB, Konopacky QM, Barman T, Macintosh B, Hoch KKW, De Rosa RJ, Wang JJ, Czekala I and Marois C (2021), Dec. Deep Exploration of the Planets HR 8799 b, c, and d with Moderate-resolution Spectroscopy. *Astron. J.* 162 (6), 290. doi:10.3847/1538-3881/ac273a. 2109.07614.
- Sallum S, Follette KB, Eisner JA, Close LM, Hinz P, Kratter K, Males J, Skemer A, Macintosh B, Tuthill P, Bailey V, DeFrère D, Morzinski K, Rodigas T, Spalding E, Vaz A and Weinberger AJ (2015), Nov. Accreting protoplanets in the LkCa 15 transition disk. *Nature* 527 (7578): 342–344. doi:10.1038/nature15761. 1511.07456.
- Sissa E, Gratton R, Garufi A, Rigliaco E, Zurlo A, Mesa D, Langlois M, de Boer J, Desidera S, Ginski C, Lagrange AM, Maire AL, Vigan A, Dima M, Antichi J, Baruffolo A, Bazzon A, Benisty M, Beuzit JL, Biller B, Boccaletti A, Bonavita M, Bonnefoy M, Brandner W, Bruno P, Buenzli E, Cascone E, Chauvin G, Cheetham A, Claudi RU, Cudel M, De Caprio V, Dominik C, Fantinel D, Farisato G, Feldt M, Fontanive C, Galicher R, Giro E, Hagelberg J, Incorvaia S, Janson M, Kasper M, Keppler M, Kopytova T, Lagadec E, Lannier J, Lazzoni C, LeCoroller H, Lessio L, Ligi R, Marzari F, Menard F, Meyer MR, Mouillet D, Peretti S, Perrot C, Potiron PJ, Rouan D, Salasnich B, Salter G, Samland M, Schmidt T, Scuderi S and Wildi F (2018), Nov. High-contrast study of the candidate planets and protoplanetary disk around HD 100546. *Astron. & Astrophys.* 619, A160. doi:10.1051/0004-6361/201732332. 1809.01001.
- Skemer AJ, Hinz PM, Esposito S, Burrows A, Leisenring J, Skrutskie M, Desidera S, Mesa D, Arcidiacono C, Mannucci F, Rodigas TJ, Close L, McCarthy D, Kulesa C, Agapito G, Apai D, Argomedo J, Bailey V, Boutsia K, Briguglio R, Brusa G, Busoni L, Claudi R, Eisner J, Fini L, Follette KB, Garnavich P, Gratton R, Guerra JC, Hill JM, Hoffmann WF, Jones T, Krejny M, Males J, Masciadri E, Meyer MR, Miller DL, Morzinski K, Nelson M, Pinna E, Puglisi A, Quanz SP, Quiros-Pacheco F, Riccardi A, Stefanini P, Vaitheeswaran V, Wilson JC and Xompero M (2012), Jul. First Light LBT AO Images of HR 8799 bcde at 1.6 and 3.3 μm : New Discrepancies between Young Planets and Old Brown Dwarfs. *Astrophys. J.* 753, 14. doi:10.1088/0004-637X/753/1/14. 1203.2615.
- Soummer R, Ferrari A, Aime C and Jolissaint L (2007), Nov. Speckle Noise and Dynamic Range in Coronagraphic Images. *Astrophys. J.* 669 (1): 642–656. doi:10.1086/520913. 0706.1739.
- Spiegel DS and Burrows A (2012), Feb. Spectral and Photometric Diagnostics of Giant Planet Formation Scenarios. *Astrophys. J.* 745 (2), 174. doi:10.1088/0004-637X/745/2/174. 1108.5172.
- Spiegel DS, Burrows A and Milsom JA (2011), Jan. The Deuterium-burning Mass Limit for Brown Dwarfs and Giant Planets. *Astrophys. J.* 727 (1), 57. doi:10.1088/0004-637X/727/1/57. 1008.5150.
- Stadler J, Benisty M, Izquierdo A, Facchini S, Teague R, Kurtovic N, Pinilla P, Bae J, Ansdell M, Loomis R, Mayama S, Perez LM and Testi L (2023), Feb. A kinematically detected planet candidate in a transition disk. *Astron. & Astrophys.* 670, L1. doi:10.1051/0004-6361/202245381. 2301.01684.
- Sudol JJ and Haghighipour N (2012), Aug. High-mass, Four-planet Configurations for HR 8799: Constraining the Orbital Inclination and Age of the System. *Astrophys. J.* 755 (1), 38. doi:10.1088/0004-637X/755/1/38. 1201.0561.
- Tanaka H, Takeuchi T and Ward WR (2002), Feb. Three-Dimensional Interaction between a Planet and an Isothermal Gaseous Disk. I. Corotation and Lindblad Torques and Planet Migration. *Astrophys. J.* 565 (2): 1257–1274. doi:10.1086/324713.
- Thalmann C, Janson M, Garufi A, Boccaletti A, Quanz SP, Sissa E, Gratton R, Salter G, Benisty M, Bonnefoy M, Chauvin G, Daemgen S, Desidera S, Dominik C, Engler N, Feldt M, Henning T, Lagrange AM, Langlois M, Lannier J, Le Coroller H, Ligi R, Ménard F, Mesa D, Meyer MR, Mulders GD, Olofsson J, Pinte C, Schmid HM, Vigan A and Zurlo A (2016), Sep. Resolving the Planet-hosting Inner Regions of the LkCa 15 Disk. *Astrophys. J. Lett.* 828 (2), L17. doi:10.3847/2041-8205/828/2/L17. 1608.08642.
- Todorov K, Luhman KL and McLeod KK (2010), May. Discovery of a Planetary-mass Companion to a Brown Dwarf in Taurus. *Astrophys. J. Lett.* 714: L84–L88. doi:10.1088/2041-8205/714/1/L84. 1004.0539.
- Toomre A (1964), May. On the gravitational stability of a disk of stars. *Astrophys. J.* 139: 1217–1238. doi:10.1086/147861.
- van Holstein RG, Girard JH, de Boer J, Snik F, Milli J, Stam DM, Ginski C, Mouillet D, Wahhaj Z, Schmid HM, Keller CU, Langlois M, Dohlen K, Vigan A, Pohl A, Carbillet M, Fantinel D, Maurel D, Origné A, Petit C, Ramos J, Rigal F, Rigalet A, Le Coroller H, Dominik C, Henning T, Lagadec E, Ménard F, Turatto M, Udry S, Chauvin G, Feldt M and Beuzit JL (2020), Jan. Polarimetric imaging mode of VLT/SPHERE/IRDIS. II. Characterization and correction of instrumental polarization effects. *Astron. & Astrophys.* 633, A64. doi:10.1051/0004-6361/201834996. 1909.13108.
- van Leeuwen F (2007), Nov. Validation of the new Hipparcos reduction. *Astron. & Astrophys.* 474 (2): 653–664. doi:10.1051/0004-6361:20078357. 0708.1752.
- Vigan A, Bonnefoy M, Ginski C, Beust H, Galicher R, Janson M, Baudino JL, Buenzli E, Hagelberg J, D'Orazi V, Desidera S, Maire AL, Gratton R, Sauvage JF, Chauvin G, Thalmann C, Malo L, Salter G, Zurlo A, Antichi J, Baruffolo A, Baudoz P, Blanchard P, Boccaletti A, Beuzit JL,

- Carle M, Claudi R, Costille A, Delboulb e A, Dohlen K, Dominik C, Feldt M, Fusco T, Gluck L, Girard J, Giro E, Gry C, Henning T, Hubin N, Hugot E, Jaquet M, Kasper M, Lagrange AM, Langlois M, Le Mignant D, Llored M, Madec F, Martinez P, Mawet D, Mesa D, Milli J, Mouillet D, Moulin T, Moutou C, Orign e A, Pavlov A, Perret D, Petit C, Pragt J, Puget P, Rabou P, Rochat S, Roelfsema R, Salasnich B, Schmid HM, Sevin A, Siebenmorgen R, Smette A, Stadler E, Suarez M, Turatto M, Udry S, Vakili F, Wahhaj Z, Weber L and Wildi F (2016), Mar. First light of the VLT planet finder SPHERE. I. Detection and characterization of the substellar companion GJ 758 B. *Astron. & Astrophys.* 587, A55. doi:10.1051/0004-6361/201526465. 1511.04076.
- Vigan A, Fontanive C, Meyer M, Biller B, Bonavita M, Feldt M, Desidera S, Marleau GD, Emsenhuber A, Galicher R, Rice K, Forgan D, Mordasini C, Gratton R, Le Coroller H, Maire AL, Cantalloube F, Chauvin G, Cheetham A, Hagelberg J, Lagrange AM, Langlois M, Bonnefoy M, Beuzit JL, Boccaletti A, D'Orazi V, Delorme P, Dominik C, Henning T, Janson M, Lagadec E, Lazzoni C, Ligi R, Menard F, Mesa D, Messina S, Moutou C, M uller A, Perrot C, Samland M, Schmid HM, Schmidt T, Sissa E, Turatto M, Udry S, Zurlo A, Abe L, Antichi J, Asensio-Torres R, Baruffolo A, Baudoz P, Baudrand J, Bazzon A, Blanchard P, Bohn AJ, Brown Sevilla S, Carillet M, Carle M, Cascone E, Charton J, Claudi R, Costille A, De Caprio V, Delboulb e A, Dohlen K, Engler N, Fantinel D, Feautrier P, Fusco T, Gigan P, Girard JH, Giro E, Gislis D, Gluck L, Gry C, Hubin N, Hugot E, Jaquet M, Kasper M, Le Mignant D, Llored M, Madec F, Magnard Y, Martinez P, Maurel D, M oller-Nilsson O, Mouillet D, Moulin T, Orign e A, Pavlov A, Perret D, Petit C, Pragt J, Puget P, Rabou P, Ramos J, Rickman EL, Rigal F, Rochat S, Roelfsema R, Rousset G, Roux A, Salasnich B, Sauvage JF, Sevin A, Soenke C, Stadler E, Suarez M, Wahhaj Z, Weber L and Wildi F (2021), Jul. The SPHERE infrared survey for exoplanets (SHINE). III. The demographics of young giant exoplanets below 300 au with SPHERE. *Astron. & Astrophys.* 651, A72. doi:10.1051/0004-6361/202038107. 2007.06573.
- Wagner K, Follette KB, Close LM, Apai D, Gibbs A, Keppler M, M uller A, Henning T, Kasper M, Wu YL, Long J, Males J, Morzinski K and McClure M (2018), Aug. Magellan Adaptive Optics Imaging of PDS 70: Measuring the Mass Accretion Rate of a Young Giant Planet within a Gapped Disk. *Astrophys. J. Lett.* 863 (1), L8. doi:10.3847/2041-8213/aad695. 1807.10766.
- Wagner K, Stone J, Skemer C, Cieza L, Dong R, Apai D, Spalding E, Leisenring J, Sitko M, Kratter K, Barman T, Marley M, Miles B, Boccaletti A, Assani K, Bayyari A, Uyama T, Woodward CE, Hinz P, Briesemeister Z, Lawson K, M enard F, Pantin E, Russell RW, Skrutskie M and Wisniewski J (2023), Oct. Direct images and spectroscopy of a giant protoplanet driving spiral arms in MWC 758. *Nature Astronomy* 7: 1208–1217. doi:10.1038/s41550-023-02028-3. 2307.04021.
- Wahhaj Z, Milli J, Romero C, Cieza L, Zurlo A, Vigan A, Pe a E, Valdes G, Cantalloube F, Girard J and Pantoja B (2021), Apr. A search for a fifth planet around HR 8799 using the star-hopping RDI technique at VLT/SPHERE. *Astron. & Astrophys.* 648, A26. doi:10.1051/0004-6361/202038794. 2101.08268.
- Wang JJ, Graham JR, Dawson R, Fabrycky D, De Rosa RJ, Pueyo L, Konopacky Q, Macintosh B, Marois C, Chiang E, Ammons SM, Arriaga P, Bailey VP, Barman T, Bulger J, Chilcote J, Cotten T, Doyon R, Duch ene G, Esposito TM, Fitzgerald MP, Follette KB, Gerard BL, Goodsell SJ, Greenbaum AZ, Hibon P, Hung LW, Ingraham P, Kalas P, Larkin JE, Maire J, Marchis F, Marley MS, Metchev S, Millar-Blanchaer MA, Nielsen EL, Oppenheimer R, Palmer D, Patience J, Perrin M, Poyneer L, Rajan A, Rameau J, Rantaky r  FT, Ruffio JB, Savransky D, Schneider AC, Sivaramakrishnan A, Song I, Soummer R, Thomas S, Wallace JK, Ward-Duong K, Wiktorowicz S and Wolff S (2018), Nov. Dynamical Constraints on the HR 8799 Planets with GPI. *Astron. J.* 156 (5), 192. doi:10.3847/1538-3881/aac150. 1809.04107.
- Wang JJ, Gao P, Chilcote J, Lozi J, Guyon O, Marois C, De Rosa RJ, Sahoo A, Groff TD, Vievard S, Jovanovic N, Greenbaum AZ and Macintosh B (2022), Oct. Atmospheric Monitoring and Precise Spectroscopy of the HR 8799 Planets with SCEXAO/CHARIS. *Astron. J.* 164 (4), 143. doi:10.3847/1538-3881/ac8984. 2208.05594.
- Weber P, P erez S, Zurlo A, Milej J, Hales A, Cieza L, Principe D, C arcamo M, Garufi A, K osp al  , Takami M, Kastner J, Zhu Z and Williams J (2023), Jul. Spirals and Clumps in V960 Mon: Signs of Planet Formation via Gravitational Instability around an FU Ori Star? *Astrophys. J. Lett.* 952 (1), L17. doi:10.3847/2041-8213/ace186. 2307.13433.
- Xie C, Choquet E, Vigan A, Cantalloube F, Benisty M, Boccaletti A, Bonnefoy M, Desgrange C, Garufi A, Girard J, Hagelberg J, Janson M, Kenworthy M, Lagrange AM, Langlois M, Menard F and Zurlo A (2022), Oct. Reference-star differential imaging on SPHERE/IRDIS. *Astron. & Astrophys.* 666, A32. doi:10.1051/0004-6361/202243379. 2208.07915.
- Zhang Z, Liu MC, Claytor ZR, Best WMJ, Dupuy TJ and Siverd RJ (2021), Aug. The Second Discovery from the COCONUTS Program: A Cold Wide-orbit Exoplanet around a Young Field M Dwarf at 10.9 pc. *Astrophys. J. Lett.* 916 (2), L11. doi:10.3847/2041-8213/ac1123. 2107.02805.
- Zhu Z, Ju W and Stone JM (2016), Dec. Shock-driven Accretion in Circumplanetary Disks: Observables and Satellite Formation. *Astrophys. J.* 832 (2), 193. doi:10.3847/0004-637X/832/2/193. 1609.09250.
- Zurlo A, Vigan A, Galicher R, Maire AL, Mesa D, Gratton R, Chauvin G, Kasper M, Moutou C, Bonnefoy M, Desidera S, Abe L, Apai D, Baruffolo A, Baudoz P, Baudrand J, Beuzit JL, Blancard P, Boccaletti A, Cantalloube F, Carle M, Cascone E, Charton J, Claudi RU, Costille A, de Caprio V, Dohlen K, Dominik C, Fantinel D, Feautrier P, Feldt M, Fusco T, Gigan P, Girard JH, Gislis D, Gluck L, Gry C, Henning T, Hugot E, Janson M, Jaquet M, Lagrange AM, Langlois M, Llored M, Madec F, Magnard Y, Martinez P, Maurel D, Mawet D, Meyer MR, Milli J, Moeller-Nilsson O, Mouillet D, Orign e A, Pavlov A, Petit C, Puget P, Quanz SP, Rabou P, Ramos J, Rousset G, Roux A, Salasnich B, Salter G, Sauvage JF, Schmid HM, Soenke C, Stadler E, Suarez M, Turatto M, Udry S, Vakili F, Wahhaj Z, Wildi F and Antichi J (2016), Mar. First light of the VLT planet finder SPHERE. III. New spectrophotometry and astrometry of the HR 8799 exoplanetary system. *Astron. & Astrophys.* 587, A57. doi:10.1051/0004-6361/201526835. 1511.04083.
- Zurlo A, Cugno G, Montesinos M, Perez S, Canovas H, Casassus S, Christiaens V, Cieza L and Huelamo N (2020), Jan. The widest H α survey of accreting protoplanets around nearby transition disks. *Astron. & Astrophys.* 633, A119. doi:10.1051/0004-6361/201936891. 1912.04911.
- Zurlo A, Go dziewski K, Lazzoni C, Mesa D, Nogueira P, Desidera S, Gratton R, Marzari F, Langlois M, Pinna E, Chauvin G, Delorme P, Girard JH, Hagelberg J, Henning T, Janson M, Rickman E, Kervella P, Avenhaus H, Bhowmik T, Biller B, Boccaletti A, Bonaglia M, Bonavita M, Bonnefoy M, Cantalloube F, Cheetham A, Claudi R, D'Orazi V, Feldt M, Galicher R, Ghose E, Lagrange AM, le Coroller H, Ligi R, Kasper M, Maire AL, Medard F, Meyer M, Peretti S, Perrot C, Puglisi AT, Rossi F, Rothberg B, Schmidt T, Sissa E, Vigan A and Wahhaj Z (2022), Oct. Orbital and dynamical analysis of the system around HR 8799. New astrometric epochs from VLT/SPHERE and LBT/LUCI. *Astron. & Astrophys.* 666, A133. doi:10.1051/0004-6361/202243862. 2207.10684.